PREFACE

This volume carries the same flavor as Volume 1 in covering the theory, algorithms, and applications of level sets and deformable models in medical image analysis.

Chapter 1 describes a new approach that integrates the T-Surfaces model and isosurface generation methods within a general framework for segmentation and surface reconstruction in 3D medical images.

Chapter 2 is a study of active contour models in medical image analysis. Various issues with respect to implantation are discussed.

Chapter 3 also deals with active contours with a primary focus on the application and performance of different types of deformable models for analyzing microscopic pathology specimens.

Chapter 4 focuses on construction of the speed function of level sets as applied to segmentation of tagged MR images.

Chapter 5 presents a parallel computational method for 3D image segmentation based on solving the Riemannian mean curvature flow of graphs. The method is applied to segmentation of 3D echocardiographic images.

Chapter 6 provides a review of the level set method and shows the usage of shape models for segmentation of objects in 2D and 3D within a level set framework via regional information.

Chapter 7 also deals with basic application of deformable models to image segmentation. Various applications of the method are presented.

Chapter 8 employs geometric deformable models/level sets to extract the topology of the shape of breast tumors. Using this framework, several features of breast tumors are extracted and subsequently used for classification of breast disease.

Chapter 9 examines various theoretical and algorithmic details of active contour models and their use for image segmentation.

Chapter 10 uses deformable models to devise a segmentation approach for ultrasound images for the study of prostate cancer.

Chapter 11 proposes a novel variational formulation for brain MRI segmentation that uses J-divergence (symmetrized Kullback-Leibler divergence) to measure the dissimilarity between local and global regions.

Chapter 12 examines the use of shape transformations for morphometric analysis in the brain. A shape transformation is a spatial map that adapts an individual's brain anatomy to that of another.

Chapter 13 proposes a nonlinear statistical shape model for level set segmentation. Various algorithmic details are provided to show the effectiveness of the approach.

Chapter 14 uses the level sets methods for structural analysis of brain white and gray matter in normal and dyslexic people.

Chapter 15 describes an approach for estimating left- and right-ventricular deformation from tagged cardiac magnetic resonance imaging using volumetric deformable models constructed from nonuniform rational B-splines (NURBS).

Chapter 16 is a generalization of the methods presented in Chapter 14 with an emphasis on autism. The 3D distance map is used as a shape descriptor of the white matter, and a novel nonrigid registration approach is used to quantify changes in the corpus callosum of normal and autistic individuals.

Overall, the thirty-one chapters in the two volumes provide an elegant cross-section of the theory and application of variational and PDE approaches in medical image analysis. Graduate students and researchers at various levels of familiarity with these techniques will find the two volumes very useful for understanding the theory and algorithmic implementations. In addition, the various case studies provided demonstrate the power of these techniques in clinical applications.

The editors of the two volumes once again express their deep appreciation to the staff at Springer who made this project a fruitful experience.

Jasjit Suri and Aly Farag
January 2007

2

PARAMETRIC CONTOUR MODEL IN MEDICAL IMAGE SEGMENTATION

Bipul Das

Imaging Technology Division, GE India Technology Centre, Bangalore, India

Swapna Banerjee

Department of Electronics and ECE, Indian Institute of Technology, Kharagpur India

The model-based technique offers a unique and efficient approach toward medical image segmentation and analysis due to its power to unify image information within a physical framework. Of the model-based techniques, the deformable model is most effectively used for its ability to unify image statistics — both local and global — in a geometrically constrained framework. The geometric constraint imparts a compact form of shape information. This chapter reviews one of the most promising and highly used deformable approaches: the active contour model in medical image analysis. The active contour model is one of the most effective approaches due to its flexibility to adapt to various anatomical shapes while constraining the local geometric shape constraint. Within the geometric paradigm, local image statistics and regional information has been effectively used in segmentation purposes. In addition, various forms of a-priori information can be incorporated into this model. Active contour models are capable of accommodating a wide range of shape variability over time and space. The active contour also has to overcome the limitation of topological adaptibility by introducing a topology adaptive model. This chapter details the development and evolution of the active contour model with the growing sophistication of medical images.

Address all correspondence to: Bipul Das, Imaging Technology Division, John F. Welch Technology Centre, GE India Technology Centre, Plot #122, Export Promotion Industrial Park, Phase 2, Hoodi Village, Whitefield Road, Bangalore 560066, India. Phone: +91 (80) 2503 3225; Fax: +91 (80) 2525 5492. bipul.das@ge.com.

1. INTRODUCTION

The rapid development and proliferation of medical imaging technologies is revolutionizing medicine. Physicians and scientists noninvasively gather potentially life-saving anatomical information using the images obtained from these imaging devices. The need for identification and interaction with anatomical tissues by physiologists has led to an immense research effort into a wide range of medical imaging modalities. The intent of medical image analysis is manifold, ranging from interpretation, analysis, and visualization to a means for surgical planning and simulation, postoperative progression of the disease, and intraoperative navigation. For example, ascertaining the detailed shape and organization of the aortic arch in the abdomen for an aneurysm operation enables a surgeon preoperatively to plan an optimal stent design and other characteristics for the aorta.

Each of the imaging modalities captures a unique tissue property. Magnetic resonance imaging (MRI) uses the heterogeneous magnetic property of tissue to generate the image [1]. The response to an applied magnetic field is distinctive for each tissue and is reflected in the image. Doppler ultrasound, on the other hand, relies on the acoustic scattering property of each tissue [2]. X-ray and computed tomography (CT) imaging [3] are based on absorption. Functional imaging modalities like positron emission tomography (PET) and fMRI (functional MRI) highlight metabolic activities in the region of interest [4–6].

Although modern imaging devices provide exceptional views of internal anatomy as well as functional images, accurate quantification and analysis of the region of interest still remains a major challenge. Physicians manually segment and analyze the images, which is highly time consuming and prone to inter-observer variability. Accurate, reproducible quantification of medical images is required in order to support biomedical investigations and clinical activities. As imaging devices are moving toward higher-resolution images and the field of view (FOV) is increasing, the size of datasets is exploding. Manual analysis is becoming more challenging and nearly impossible. Thus, the need for computer-aided automated and semi-automated algorithms for segmenting and analyzing medical data is gaining importance.

The variability of anatomic shapes makes it difficult to construct a unique and compact geometric model for representation of an anatomic region. Furthermore, many factors contribute to degradation of image quality, which makes the process of segmentation even more challenging. Although the nature of artifacts may vary with imaging modality and the tissue concerned, their effect on image quality is nevertheless detrimental. Figures 1 and 2 the illustrate effects of two different types of artifacts in the process of image acquisition. In Figure 1 the inhomogeneity factor makes the middle region of the image darker compared to the top and lower side. In this case the inhomogeneity factor is a slowly varying intensity gradient

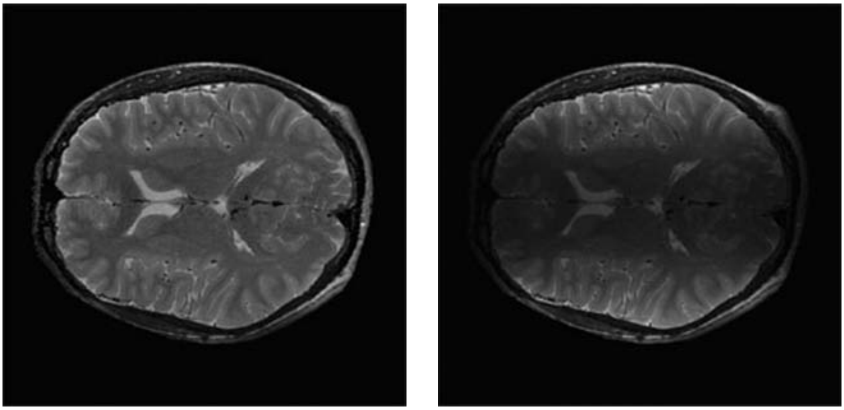

(a) (b)

Figure 1. Effects of inhomogeneity in MRI images of brain: (a) images without inhomogeneity; (b) with inhomogeneity effects.

Figure 2. Illustration of streak artifacts in CT images.

from the middle to the outer sides. Figure 2 shows the effect of metal in CT, where radial streaks are observed from the metal sites (right region in the image).

The resolution of the imaging device also determines image quality. A low-resolution device suffers from problems of fuzzification and occlusion of boundaries, giving rise to blurred and disconnected anatomical edges. But an increase in image resolution is limited by factors like a low signal-to-noise ratio, exposure to more radiation, extended imaging time, and increasing contrast dosages. With all these factors affecting image quality, the challenge for the image analysis community is to find suitable algorithms to accurately and reproducibly segment anatomical structures for clinical studies.

Traditional low-level image processing techniques perform operations using local image statistics, producing localized patterns that need unification to form a meaningful segmentation. However, in most cases it leads to incorrect connected boundaries due to a lack of sufficient statistics in most regions. Moreover, the above-mentioned artifacts immensely bias the local statistics, making it impossible to generate anatomically correct structures. As a result, these techniques require a considerable amount of manual intervention to generate a meaningful structure, making it a tedious process, and one prone to operator subjectivity.

On the other hand, the use of global properties like intensity values or compact geometric models is also not always possible since these properties themselves do not necessarily have a one-on-one mapping with an anatomical structure or a desired region of interest. A methodology that can encapsulate local statistics in a global framework might prove to be a better alternative in this respect. Deformable models [7–11] comprise a step in that direction. The main idea of these models is that of using local statistics to deform a global geometric model. Through the last two decades, deformable models have been a promising and vigorously researched approach to computer-assisted medical image analysis. The source of the immense potential for the use of deformable models in segmentation, matching, and tracking of anatomic structures in medical images lies in its bottom–up approach, which exploits features derived from local image statistics along with a priori knowledge about the location, size, and shape of these structures [12]. This allows a high range of variability of these models to accommodate significant variation in biological structures.

The active contour model, commonly known as the snakes model, proposed by Kass et al. [10], defines a parametric framework for a curve that deforms under the action of local image statistics to conform into the perceived boundary of the structure in an image. For the last two decades, the active contour model has found widespread application in many fields of medical image segmentation and has undergone immense development in terms of its theoretical insight, as well as making itself more flexible and adaptable. This chapter tries to capture the evolution of this model and its use in medical image segmentation. Organization of the chapter is as follows: Section 2 provides the basic theory of an active contour and explains the underlying physics. The confluence of geometry and image properties is also explained in this section and the effects of each of the properties are explored. Section 3 describes the evolution of the snake model to address the requirements of medical image analysis applications. Section 4 describes the inclusion of a-priori information within the snake framework. Section 5 deals with the topological adaptability of the snake. We conclude with some discussion in Section 6.

2. ACTIVE CONTOUR MODEL: THEORY

This section will elaborate the theory of the active contour model. For easy reference, the definitions and notations used here are defined in the next subsection.

2.1. Definitions and Notations

We use $\Re$ is to denote a real number line, and $\Re^2$ will denote the Euclidean plane. An *image* is considered to be embedded on a rectangular subspace $R \subset \Re^2$. Over R, intensity values are acquired at every point with integral coordinates commonly referred to as *pixels*. A point in R will be represented as a two-dimensional position vector $\mathbf{u} = (x, y)$, where x, y denote the x- and y-coordinate values of $\mathbf{u}$. Let $f : R \rightarrow [0, 1, 2, 3, ..., \text{MaxIntensity}]$ denote the *intensity function* for a given image.

A *parametric curve* or *spline* is represented as a function $\boldsymbol{\tau} : [0, 1] \rightarrow \Re^2$. A curve is closed if the initial and terminal points are identical, i.e., $\boldsymbol{\tau}(0) = \boldsymbol{\tau}(1)$. A point on the curve will be denoted by $\boldsymbol{\tau}(s) = (x(s), y(s))$, where $s \in [0, 1]$ denotes the arc-length parameter, and $x(s)$ and $y(s)$ refer to its location in the xy-plane. Although in a continuous space any real value in $[0, 1]$ may be assigned to the parameter s, in the digital world only discrete values can be used. The snake is an ordered sequence of discrete points on a curve at a regular interval $\delta < 1.0$, where δ is a finitely small positive number. The points ..., $\boldsymbol{\tau}(-2\delta), \boldsymbol{\tau}(-\delta), \boldsymbol{\tau}(0), \boldsymbol{\tau}(\delta), \boldsymbol{\tau}(2\delta), ...$ on a snake $\boldsymbol{\tau}$ at an interval of δ will be referred to as *control points*.

Let a contiguous set of pixels belonging to the structure of interest, sharing some similar attributes, be called the *foreground* and be denoted as $O \subset R$, where R is the image space. Any pixel $c \in O$ is called an object pixel. On the other hand, any pixel $c \in R - O$, i.e., belonging to the image space R but not belonging to the object space O, is a *background* pixel. The task of image segmentation is to identify the foreground O from the image space R. This requires representation of the foreground region into a compact geometric form.

2.2. Basic Snake Theory

Snakes are planar deformable contours that are useful in several image analysis tasks. In many images, the boundaries are not well delineated due to degradation by regional blurring, noise, and other artifacts. Despite these difficulties, human vision and perception interpolate between missing boundary segments. An active contour model is intended at inculcating this property of the human vision system. So the snake framework is formulated such that it approximates the locations and shapes of object boundaries in images based on the assumption that boundaries are piecewise continuous or smooth.

The mathematical basis for active contour models owes its foundation to the principle of unification of physics and optimization theory [12]. The laws of physics define the underlying principle of how a geometrical shape can vary over space and time. An active contour model permits an arbitrary shape to evolve to a meaningful shape guided by the image properties and constrained by the physical laws. The physical laws provide the desired intuitive nature to the evolving shape. In particular, for the snake, the points does not evolve independently but are constrained by the motion of the two nearest points on either side, thus confining its degrees of freedom, bringing an elastic model into the structure. Thus, it evolves from the elastic theory paradigm, generally in a Lagrangian dynamics setting. It stems from the theory of an elastic string deforming naturally to applied forces and constraints defined by various sources.

Guided by the physical laws, the model is driven to deform toward a lower-energy or equilibrium state monotonically. The local image statistics should be formulated within the deformable paradigm in such a way that the model is guided to delineate the desired anatomic structure. The optimization theory blends these two different forms of constraints within the same framework. The local image statistics-based features thus need to be defined within the framework of this physics-based geometric model, such that the "equilibrium state" is achieved only when the anatomic structure is delineated.

Definition of this physics-based model that governs the deformation property of the string is the main essence that makes the deformable model an attractive proposition to capture the local statistics of the image globally. A deformable model, and in particular an active contour model, by definition optimally integrates similar salient features within the geometric model.

The active contour model, or snake, proposed by Kass et al. [10] is an elastic contour that deforms under the guidance of attributed geometric and image properties. This phenomenon of deformation, as guided by physical laws, is defined in terms of an energy minimization framework. By definition, it is minimization of the total energy over the entire shape, defined by

$$E_{\text{snake}}(\boldsymbol{\tau}) = E_{\text{int}}(\boldsymbol{\tau}) + E_{\text{ext}}(\boldsymbol{\tau}) \tag{1}$$

where $E_{\text{snake}}(\boldsymbol{\tau})$ is the total energy of the contour $\boldsymbol{\tau}$, composed of the internal energy $E_{\text{int}}(\boldsymbol{\tau})$ and external energy $E_{\text{ext}}(\boldsymbol{\tau})$. Internal energy is defined by the physical constraints that describe the degrees of freedom of the contour $\boldsymbol{\tau}(s)$, and the external energy is defined by the image properties and other user constraints (e.g., landmark).

As defined previously, the physical constraints of the active contour model have their origin in the physics of an elastic body, which is described in the first term of the functional in Eq. (1). The internal energy term can be expressed as

$$E_{\text{int}}(\boldsymbol{\tau}) = \int_0^1 \left[\alpha(s) \left| \frac{\partial \boldsymbol{\tau}(s)}{\partial s} \right|^2 + \beta(s) \left| \frac{\partial^2 \boldsymbol{\tau}(s)}{\partial s^2} \right|^2 \right] ds, \tag{2}$$

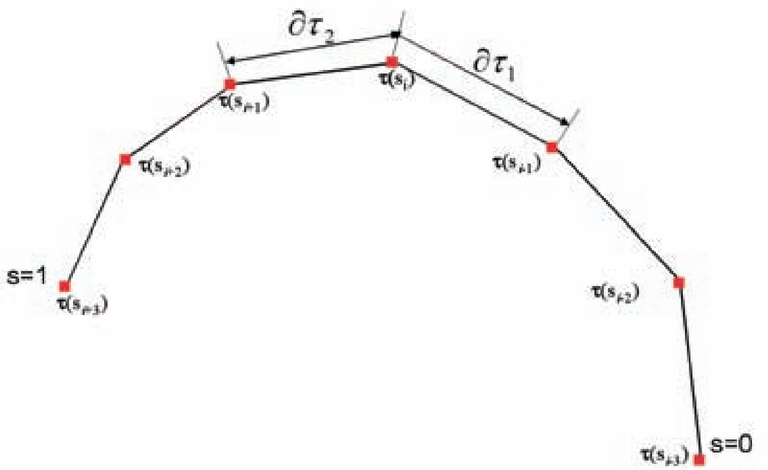

Figure 3. Illustration of computation of the surface tension and rigidity energies in the parametric snake framework. See attached CD for color version.

where the first term simulates the tension of the contour and the second, which is in essence the acceleration term, simulates the rigidity of the contour $\boldsymbol{\tau}(s)$. $\alpha(s)$ and $\beta(s)$ ($\alpha(s), \beta(s) \in [0,1]$) are the controlling strengths associated with the surface tension and rigidity terms. Although the strength factors are expressed as functions of the parameter s, in most cases they remain constant throughout the contour length. Thus, the term s will be dropped in future references to these factors for simplification.

Let us see how these terms control the contour behavior as the total energy functional tries to minimize itself. The first order derivative term in Eq. (2) can be minimized by reducing the value of the numerator. Thus, the difference between the two points $\partial\boldsymbol{\tau}$ needs to be reduced (see Figure 3), which leads to shrinking the length of the contour $\boldsymbol{\tau}(s)$. On the other hand, the second term in the expression is by definition the curvature term. Reduction of that term means the difference between $\partial\boldsymbol{\tau}_1$ and $\partial\boldsymbol{\tau}_2$ in Figure 3 needs to be minimized. Thus, minimizing this term leads to resistance to any bending and eventually straightening the contour $\boldsymbol{\tau}(s)$, leading to a smooth contour. In case the contour is a closed one, the effect of these two terms will lead to a shrinking circle, in the absence of any other force.

Once the physical constraints are defined, the behavior of the contour is well set in terms of its geometric properties. However, its behavior on the image domain needs to be controlled by the image statistics-driven factors, such that the local minima coincide with the image feature of interest. For example, when the snake needs to converge onto image edges, then the external energy function needs to be defined as $-\gamma \left|\nabla G_\sigma * I(x,y)\right|^2$, where γ controls the magnitude of the potential, ∇ is the gradient operator, and $G_\sigma * I(x,y)$ denotes the image intensity $I(x,y)$ convolved with a (Gaussian) smoothing filter whose characteristic width σ controls the spatial extent of the local minima of the convolution kernel. Note here that the expression for the edge operator has a negative sign associated with it. The reason for this is that the local minima of the contour need to coincide with the maxima of the gradient functional. Also, note that the squared magnitude has been used for the edge functional computation. A different approach is also used, where the vector form of the gradient is used instead of the scalar information. However, in the Lagrangian setting an energy expression is required for solving the minimization problem. Thus, for the vector-based approach the dot product of the contour normal with the gradient is used for defining the energy functional and is expressed as $(\nabla G_\sigma * I(x,y)) \cdot \mathbf{N}(\boldsymbol{\tau}(x(s),y(s)))$, where $\mathbf{N}(\boldsymbol{\tau}(x(s),y(s)))$ is the normal to the contour $\boldsymbol{\tau}(s)$ at location $x(s),y(s)$. Similarly, image intensity has been widely used along with edge information to formulate the external energy functional. The total external energy of the contour can be defined as

$$E_{\text{ext}}(\boldsymbol{\tau}) = \int_0^1 \mathbf{E}_{\text{ext}}(\boldsymbol{\tau}(s))ds, \tag{3}$$

where $\mathbf{E}_{\text{ext}}(\boldsymbol{\tau}(s))$ denotes the energy functional given by the image properties at the point $\boldsymbol{\tau}(s)$.

In summary, the basic definition of deformable parametric curve contains two terms: (a) internal energy, which defines the geometric properties of the curve; and (b) external energy, which combines all other forces that guide the curve to delineate the desired structure. Once the basic energy formulation is done, the idea is to find a methodology for energy minimization. A number of approaches have been proposed so far for energy minimization of the contour. The most well known is by solving the partial differential equation (PDE) for force (defined through an Euler-Lagrangian) using a finite-difference [10] or finite-element method [13]. A dynamic programming-based approach [14] and greedy snakes [15] are also used in many applications. The next subsection will briefly touch upon these approaches. Since these are quite standard ways of solving minimization problems, this chapter gives only the basic idea behind each of the methodologies. The pseudocode for the Euler-Lagrangian and greedy snakes are provided in Appendix 1.

2.3. Energy Minimization

According to the calculus of variations, the contour that minimizes the energy $E_{\text{snake}}(\boldsymbol{\tau})$ must satisfy the Euler-Lagrange equation [10]

$$\frac{\partial}{\partial s}\left(\alpha \frac{\partial \boldsymbol{\tau}(s)}{\partial s}\right) - \frac{\partial^2}{\partial s^2}\left(\beta \frac{\partial^2 \boldsymbol{\tau}(s)}{\partial s^2}\right) - \nabla \mathbf{E}_{\text{ext}}(\boldsymbol{\tau}(s)) = 0. \tag{4}$$

This can be viewed as a vector-valued partial differential equation balancing internal and external forces at equilibrium given by

$$\mathbf{F}_{\rm int} + \mathbf{F}_{\rm ext} = 0, \tag{5}$$

where $\mathbf{F}_{\rm int}$ represents the internal force due to stretching and bending factors, given by

$$\mathbf{F}_{\rm int} = \frac{\partial}{\partial s}\left(\alpha \frac{\partial \boldsymbol{\tau}(s)}{\partial s}\right) - \frac{\partial^2}{\partial s^2}\left(\beta \frac{\partial^2 \boldsymbol{\tau}(s)}{\partial s^2}\right). \tag{6}$$

The first term in Eq. (6) is the stretching force derived from the surface tension, while the second term represents the bending force. The external forces couple the contour to the image information in a way that equilibrium is accomplished when it balances with the physical constraints on the contour. Thus, $\mathbf{F}_{\rm ext}$ is expressed as

$$\mathbf{F}_{\rm ext} = -\nabla \mathbf{E}_{\rm ext}(\boldsymbol{\tau}(s)), \tag{7}$$

which pulls the contour toward the salient image features of interest. Other forces can be added to impose constraints defined by the user. We will make use of additional forces.

To solve the energy minimization problem, it is customary to construct the snake as a dynamical system that is governed by the functional to evolve the system toward equilibrium. The snake is made dynamic by treating the evolving contour $\boldsymbol{\tau}$ as a function of both time t and arc-length s. This unifies the description of shape and motion within the same framework of Lagrangian mechanics. Thus, this formulation not only captures the shape of the contour but also quantifies its evolution over time. The Lagrange equations of motion for a snake is given by

$$\mu \frac{\partial^2 \boldsymbol{\tau}(s)}{\partial t^2} + \nu \frac{\partial \boldsymbol{\tau}(s)}{\partial t} + \frac{\partial}{\partial s}\left(\alpha \frac{\partial \boldsymbol{\tau}(s)}{\partial s}\right) - \frac{\partial^2}{\partial s^2}\left(\beta \frac{\partial^2 \boldsymbol{\tau}(s)}{\partial s^2}\right) = \nabla E_{\rm ext}(\boldsymbol{\tau}(s)), \tag{8}$$

where μ is the mass constant and ν the damping density following Newton's laws of motion. The system achieves equilibrium when the internal stretching and bending forces balance with the external forces and the contour ceases to move, i.e., both the acceleration and velocity terms vanish; in other words, $\frac{\partial^2 \boldsymbol{\tau}}{\partial t^2} = \frac{\partial \boldsymbol{\tau}}{\partial t} = 0$.

For numerical solution of the equation, discretization of the equation is required. This is in general accomplished using a finite difference for solving the partial differential equation. In the discrete domain the energy equation can be expressed as

$$E(\mathbf{v}) = \frac{1}{2}\mathbf{v}\mathbf{A}\mathbf{v} + E_{\rm ext}(\mathbf{v}), \tag{9}$$

where $\mathbf{v}$ is the discretized version of the contour $\boldsymbol{\tau}(s)$, and $\mathbf{A}$ is the stiffness matrix. For all practical purposes, in this text we will use the symbol $\boldsymbol{\tau}(\delta)$ for discrete representation of the contour. Minimum energy estimation is equivalent to setting the gradient of Eq. (10) to 0, which results in the following linear equation:

$$\mathbf{A}\tau = \mathbf{F}, \tag{10}$$

where $\mathbf{A}$ is the penta-diagonal stiffness matrix, and $\boldsymbol{\tau}$ and $\mathbf{F}$ represent the position vectors $\boldsymbol{\tau}_i = \boldsymbol{\tau}(i\delta)$ and the corresponding force at these points $\mathbf{F}(\boldsymbol{\tau}_i)$, respectively.

As the energy-space cannot be ascertained to be convex, so there is a high probability of getting local minima in the energy surface. In fact, finding the global minimum of the energy is not necessarily meaningful. Indeed, the main interest is finding a good contour that optimally fits to delineate the anatomic structure of interest in the best possible manner.

A neighborhood around each control point is considered and the total energy of the contour is computed for each neighborhood. Energy minimization continues until the energy between two consecutive iterations changes. This dynamic programming approach [14] searches for global minima in the image space. Greedy snakes [15], on the other hand, searches for local minima for each of the control points. The local motion of the points is considered in the neighborhood for energy minimization. In contrast to dynamic programming [14], greedy snakes [15] minimizes the energy of each local control point. Figure 4 illustrates the neighborhood search around a control point for dynamic programming and the greedy snakes algorithm.

3. ACTIVE CONTOUR EVOLUTION

The image processing task can be broadly classified into two categories: region-based and boundary based operations. Image processing techniques like mathematical morphological operations, region growing, and other region-based operations use regional homogeneity statistics to drive the task of image processing. Boundary-based operations (e.g., edge detection, gradient computation) use the statistics of variation in a local neighborhood. Low-level image processing techniques, if used independently for the purpose of segmentation, require a high level of manual intervention, rendering the result prone to inter- and intra-operator variability.

This chapter will focus on gradient-based approaches that rely mostly on image edges for convergence. Subsequent modifications for the gradient-based approaches and challenges faced at various levels of medical image segmentation will be discussed. Eventually, incorporation of region-based forces within the snake model help in providing a more compact model for the segmentation process. Region-based information can be incorporated in many ways into the energy minimization equation.

The active contour model allows user interaction at various stages. The main intention of the active contour is to reduce the amount of user intervention in the

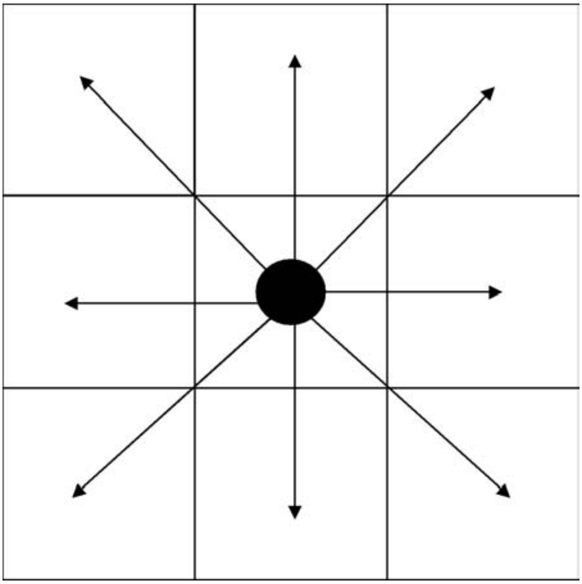

Figure 4. Neighborhood search for the minimum energy configuration.

process of segmentation. In particular, ideally, the user has to provide an initial contour near the desired edge. The snake deforms under the action of the local image forces and geometric constraints until it conforms to the final edges of the image.

The deformable model is in itself not free from limitations. In the original proposition, the user needs to provide the initial contour very near the desired edges; otherwise, the snake will not be able to deform to capture the desired anatomical structure. At the initial stage a number of solutions [17, 18] were provided in different forms to allow the snake more evolution. Cohen et al. [13] proposed a solution to propagate the contour faster toward the desired image edges. An internal pressure force was introduced by regarding the curve or surface as an inflating *balloon*. This pressure pushes the contour boundary toward the edges, and thus makes initialization of the snake a simpler process. However, the associated limitation of the snake remains in its ability to balance the strength of the balloon force with edge strength. As the balloon force is increased, there is a chance of leakage at weak edges. The addition of balloon pressure, though, adds to the propagation strength; however, this increases the instability of the snake framework. Berger et al. [18] proposed a "snake-growing" algorithm, where the snake grows based on the local contour information. Figure 6 shows the comparative result of a snake-growing compared to a conventional snake.

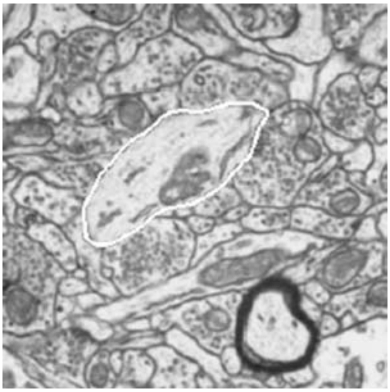

Figure 5. Illustration of segmentation of cellular structure in an EM photomicrograph. Reprinted with permission from [16]. Copyright ©1994, IEEE.

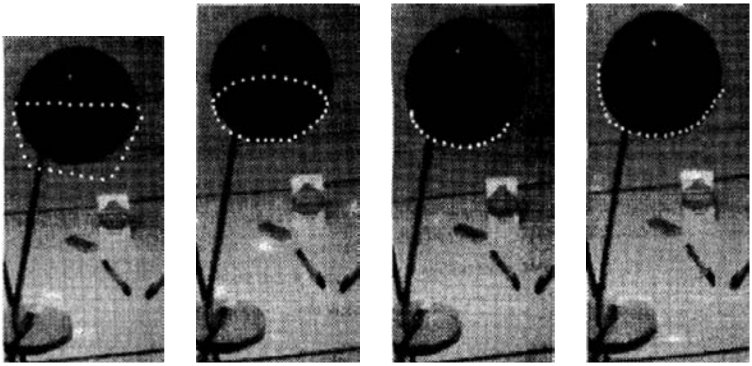

(a) (b) (c) (d)

Figure 6. Illustration of snake-growing algorithm in comparison to conventional snake. (a) Initial contour shown in white dots. (b) Result of conventional snake. (c–e) Performance of snake-growing algorithm. Reprinted with permission from [18]. Copyright ©1990, IEEE.

Leymarie and Levine [19] utilized a distance transform metric from the gradient information within the active contour framework to define a *grassfire transform*. The main motivation of the work was to define shape through skeletonization. In particular, an object's boundary is taken as the initial firefront that propagates within the interior of the object defined by the closed boundaries of the object. Points where the firefronts meet are considered the skeleton points of the representative object. The firefront propagation is accomplished using the active contour framework guiding the propagation using the distance transform from the boundaries. This work tries to bring in the gradient-based and regional informa-

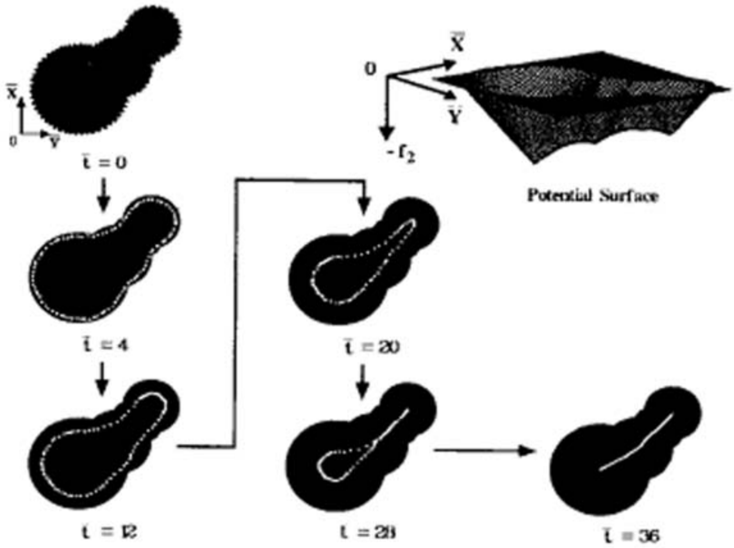

Figure 7. Example of grassfire propagation using an active contour model. The potential surface shows the valley in the distance transform function. Other images show the evolution of the snake toward the skeleton of the object. Reprinted with permission from [19]. Copyright ©1992, IEEE.

tion within the same framework to define the skeleton. However, this application has the probability of suffering from situations where noise plays a dominant role in determining the image gradient quality. Figure 7 depicts examples of skeletonization using this technique. Clearly, this formulation requires well-defined boundaries, which are absent in most medical images.

Lobregt et al. [20] tried to implicitly address the challenge due to fuzzy boundaries in medical images by controlling the local curvature of the contour in a local coordinate system. In this work, a local coordinate system was defined with respect to the vertex of the contour, and the change of curvatures in local and global coordinate system was taken into account. Thus, instead of global curvature variation, the contour deforms based on the variation in local and global curvature. This in turn retains the length of the contour, which otherwise has a shrinking property. It is important to mention that the curvature in this approach has been attributed to a direction both globally and locally. The approach intends that internal forces that act on the vertices should have the same (radial) direction as the curvature vectors. This means that internal forces can be derived from the curvature vectors by modifying only their lengths. Second, in order to reduce local curvature without affecting areas of constant curvature, the lengths of the internal force vectors

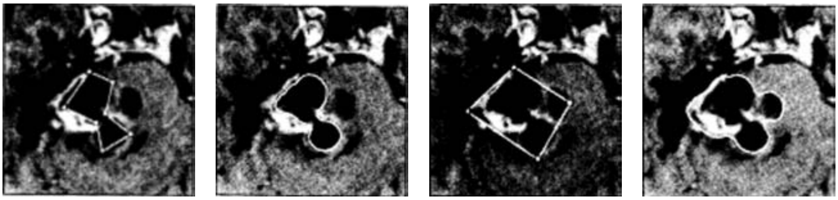

(a) (b) (c) (d)

Figure 8. Illustration of dynamic discrete contour evolution on a cropped region from an MR image of brain. (a,c) Initial contour drawn manually. (b,d) Segmentation result from the contours of (a) and (c), respectively. Reprinted with permission from [20]. Copyright ©1995, IEEE.

should be zero for parts of the contour with constant curvature. To accomplish this, the dot product of the local $\mathbf{r}_i$ and global radial vectors $\mathbf{c}_i$ at point i is computed and convolved with a discrete filter **f**. The idea here is to reduce the high-frequency component and rather retain only the DC component. Thus, the choice of filter needs to be such that the result of convolution is zero. This approach results in a smoother contour and also allows an open contour to evolve within the snake framework. Figure 8 shows the results of deformation using the dynamic discrete contour.

3.1. Gradient Orientation

A different problem arises when two strong disconnected edges come close to each other. In these cases, the strong gradient acts independently to attract the contour. The final result thus becomes dependent on a number of factors like the contour's relative location with respect to the participating edges, their strengths, and possibly on all other force factors in the neighborhood. In many cases, the resulting contour alternates between the two strong edges. Falcaõ et al. [21, 22] addressed this problem in their proposed "live-wire" framework. The "live-wire" uses the gradient orientation information to detect the "true" boundary and avoids the possibility of getting trapped by strong edges. Similarly, the gradient orientation can be used in the snake framework [23]. Instead of using the gradient force without any reference to the contour, the external energy due to the gradient can be defined by the contour orientation and gradient direction. The idea is to make the "false" boundary invisible to the contour, so that it does not snap onto the "false" edge. Here, the direction of gradient is defined as whether it is a step-down or a step-up gradient. Now, this direction depends on the point from which we are looking at the gradient and the orientation of the contour. For example, in Figure 9, if we observe the edge marked green from the blue point, it seems to be a step-down gradient, while if it is observed from the red point, the gradient is a step-up gradient.

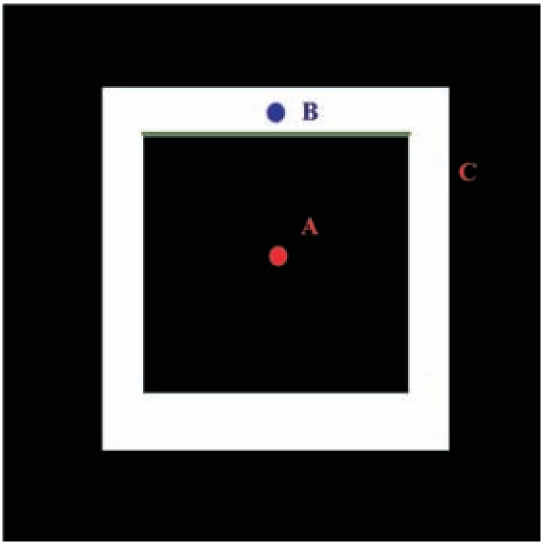

Figure 9. Illustration showing step-up and step-down edges from the observer's point of view. See attached CD for color version..

Now, if the contour approaches from the region marked A, then to track the interface between regions A and B it should latch onto a step-up edge along its outer normal. On the other hand, if it approaches from region B to the same interface, the contour point needs to snap at a step-down gradient inside the enclosed region of the contour. In other words, in the latter case the inward normal should see a step-down gradient. If the orientation of the contour is taken into account, then the desired edge would either be on the right- or left-hand side of the contour depending on whether it is considered in a clockwise or anticlockwise sense. Falcão et al. [21, 22] proposed a solution using the concept of contour orientation that relates gradient direction with the unit vector orthogonal to the local contour segment and directed from the "exterior" to the "interior".

Let $\theta_G(\boldsymbol{\tau}(s_i)) = \tan^{-1} \nabla_y f(\boldsymbol{\tau}(s_i))/\nabla_x f(\boldsymbol{\tau}(s_i))$ be the direction of the intensity gradient at the point $\boldsymbol{\tau}(s_i)$, where s_i indicates the ith control point on contour $\boldsymbol{\tau}$. $\nabla_y f(\boldsymbol{\tau}(s_i))$ and $\nabla_x f(\boldsymbol{\tau}(s_i))$ are the gradients along the y- and x-directions, respectively, at the point $\boldsymbol{\tau}(s_i)$. As previously mentioned, $f(x, y)$ denotes the image intensity at the location (x, y). If $\theta_N(\boldsymbol{\tau}(s_i))$ is the normal to the contour at $\boldsymbol{\tau}(s_i)$, then the energy due to the gradient field is defined as

$$E_{\text{gradient}}(\boldsymbol{\tau}(s_i)) = \begin{cases} -\mathbf{F}_{\text{gradient}}(\boldsymbol{\tau}(s_i)) \bullet \mathbf{N} & \text{if } |\theta_G(\tau(s_i)) - \theta_N(\tau(s_i))| \leq \frac{\pi}{2} \\ 0 & \text{otherwise} \end{cases} \tag{11}$$

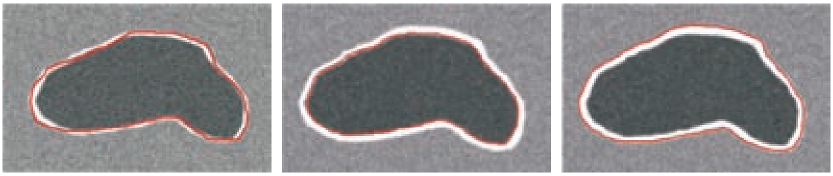

(a) (b) (c)

Figure 10. Illustration of gradient orientation on snake deformation: (a) contour deformation without gradient orientation information; (b) segmentation of region when foreground intensity is less than background and (c) when foreground intensity is greater than background intensity. In both (b) and (c) the contour has properly latched onto the desired boundary. See attached CD for color version. Reprinted with permission from [24]. Copyright ©2004, SPIE.

The normal $\theta_N(\boldsymbol{\tau}(s_i))$ at a point $\boldsymbol{\tau}(s_i)$ on the contour $\boldsymbol{\tau}$ at s_i is defined as

$$\theta_N(\tau(s_i)) = \theta_C(\boldsymbol{\tau}(s_i)) + \lambda\frac{\pi}{2}, \tag{12}$$

where $\theta_C(\boldsymbol{\tau}(s_i))$ is the tangent at the point $\boldsymbol{\tau}(s_i)$. The value of λ can be +1 or –1 depending on the desired direction of the normal. If the object intensity is greater than the background, then for contour in the counterclockwise direction the value of lambda should be 1, indicating an inward normal. This ensures that the contour will only be able to see the gradient, which is in the direction of the inward normal. But if it encounters a step-up gradient, then the difference between the two gradient angles and the growing normal will be more than $\frac{\pi}{2}$, so that the step-up gradient will be invisible to the growing contour. The reverse is the case if the contrast is changed. The effect of using the gradient orientation information within the snake framework is shown in Figure 10b,c. Snake deformation without the orientation information is illustrated in Figure 10a, which shows the final contour alternating between the two disconnected strong edges [24].

3.2. Convergence to Concavities

One of the major challenges faced in the initial phases of snake formulation was its inability to converge into concavities. Xu and Prince [25] designed a new external static force field vector $\mathbf{F}_{\text{ext}}(x, y) = \mathbf{v}(x, y)$, called the gradient vector flow field. This field originates from the edges and makes the snake converge to the gradient concavities. The gradient vector flow field is the vector field $\mathbf{v}(x, y) = [u(x, y), v(x, y)]$, which minimizes the energy functional

$$E = \iint \mu(u_x^2 + u_y^2 + v_x^2 + v_y^2) + |\nabla g|^2 \left|\mathbf{v} - \nabla g\right|^2 dxdy, \tag{13}$$

where g is the intensity gradient.

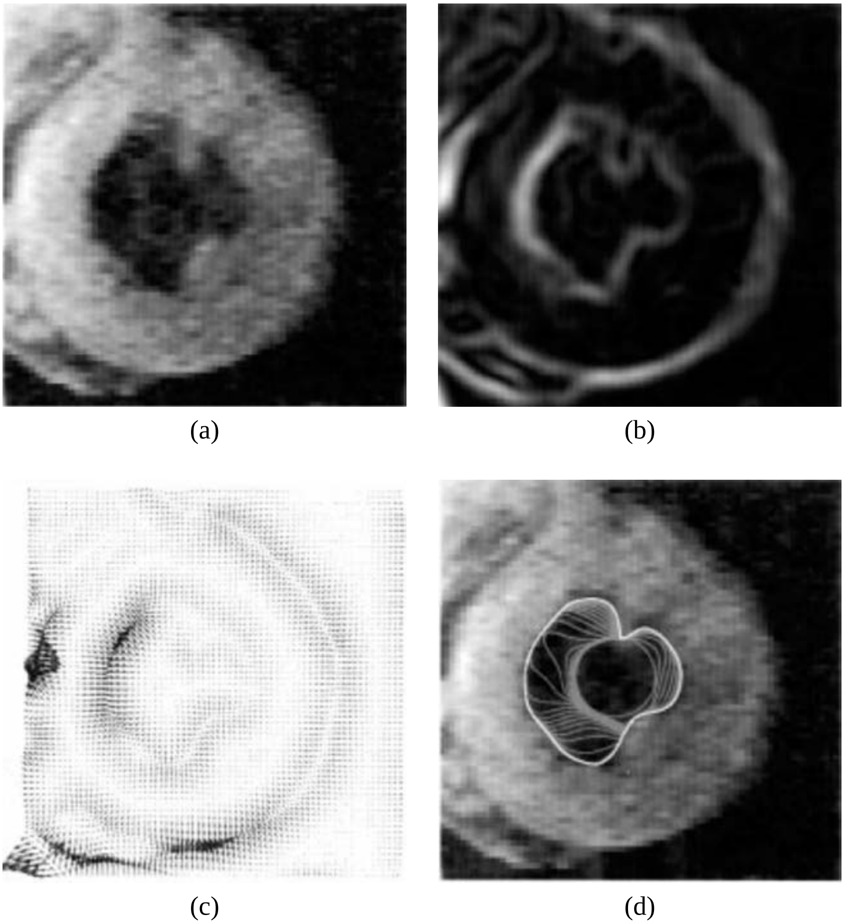

Figure 11. Illustration for performance of gradient vector flow (GVF) snake in segmentation of left ventricle from an MR image of heart: (a) original MR image showing left ventricle; (b) gradient map derived from (a); (c) vector flow field of the gradient map; (d) segmentation result using GVF snake. Reprinted with permission from [25]. Copyright ©1998, IEEE.

The basic nature of this force field is such that deformation near the nonhomogeneous regions of the image is governed by the gradient function, while in the homogeneous region the first term dominates. This results in a flow vector that converges into the edges of the image. Figure 11 illustrates the performance of gradient vector flow-based active contour model in segmentation of the left ventricle from MR images of the heart.

Anatomical structures vary widely in shape, size, and geometry. Segmentation of this wide range of anatomical structures requires highly deformable models to

(a) (b)

Figure 12. Images showing the performance of the inertial snake on (a) computer-generated phantom image and (b) ultrasound image of an artery of the lower limb [26]. See attached CD for color version.

fit into the process. As the contour itself is evolving under the effect of geometric physical constraints, the framework in its very definition imposes a geometric smoothness into it. Although this is effective in many situations, many other cases require relaxation of the physical constraints for appropriate segmentation. While in tracking geometric deformation in smooth structures the curvature is helpful, in segmentation of structures like white matter or convex structures the effect of curvature needs to be reduced. A study on the discrete computation and effect of curvature is presented in [15].

A potential way of controlling snake movement to conform into image boundaries and to avoid leaking is by incorporating an adaptable propagation force that modifies itself as it moves from a homogeneous to a nonhomogeneous region [26]. At this point, this is done by using an inertial snake, where the propagation term of active contour deformation is controlled by its distance from the initial contour. In that approach, the balloon force modifies itself and slows down at a rate directly proportional to the deformation rate between the successive iterations. Thus, in homogeneous region the force is higher, supporting faster propagation. But as the contour approaches the high-gradient region, the force reduces itself, thus discouraging propagation. The uncontrolled motion of the balloon force is thus controlled by the homogeneity and gradient information. Figure 12 illustrates the result of the inertial snake on computer-generated phantoms and ultrasound images.

Other significant attempts to improve the snake model using gradient-based information and internal energy has been pursued by other researchers [27, 28]. However, the main limitation remained its dependence on local image statistics, which is not reliable in many situations. Mostly for medical image analysis and

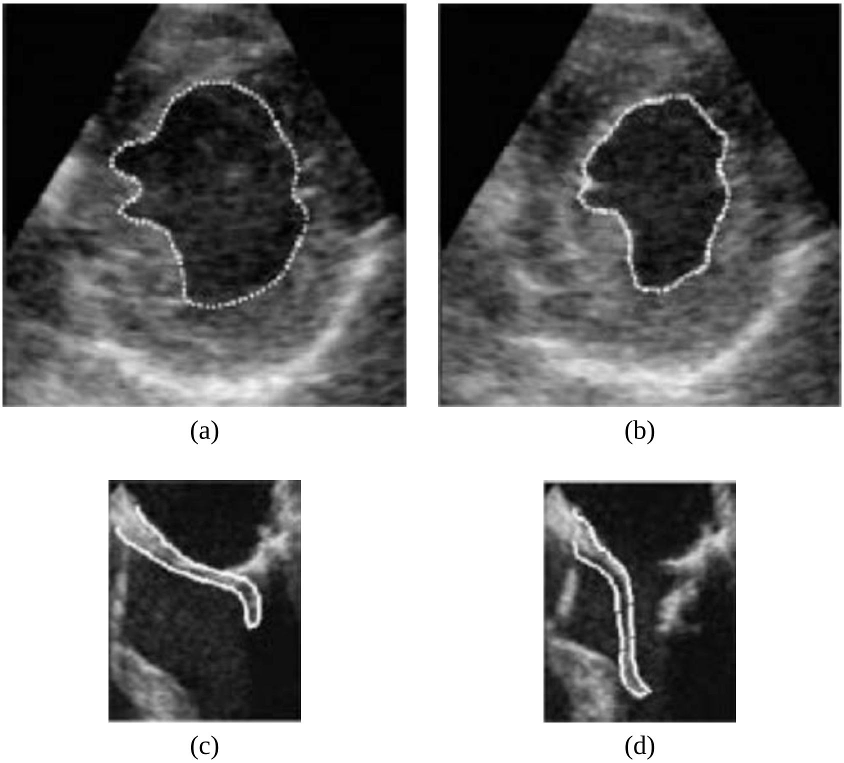

Figure 13. Images showing tracking of (a,b) endocardial boundary using the active contour model and (c,d) the mitral valve leaflet boundary. Reprinted with permission from [28]. Copyright ©1998, IEEE.

segmentation problem, one of the major challenges lies in the occurrence of fuzzy boundaries, as previously mentioned. Thus, transition from one region to another remains occluded by a lack of strong edges. Visually the transition can be observed by a change in other features and from the global information. Thus, where local statistics proved to have limitations in making a clear distinction between two regions, utilization of global statistics within the snake framework was found to be helpful.

3.3. Regional Information

Deformable models attracted the attention of the medical image analysis community for its ability to conform to the same framework constraints for a geometric shape and image information. In particular, after the introduction of regional energy that controls the propagation term, this model became more popular. The main motivation was to use global features and reduce reliance on local features. The rationale behind this approach was the fact that the features derived from local statistics are prone to errors due to noise and other artifacts that arise during the imaging process. Thus, a more global statistics would be helpful in detecting the region of interest. In fact, the basic definition of a structure can be stated as the region with similar attributes. If the features of interest can be isolated, the region connected by the similar features can be defined as the same structure. This gives rise to an entirely new approach toward the deformable model and has been studied in various forms by different researchers [29–32].

Region-based information is in general incorporated into the snake structure through a probabilistic model. As mentioned earlier, regional information attempts to capture the likelihood of a pixel (or point) belonging to any specified region. In general, the "region" is defined using some feature parameter, namely intensity, texture, etc. Based on the feature value, a pixel has a finite probability of belonging to a region defined in the feature space. The most widely used measures for feature space definition in snake-based segmentation is intensity. In some approaches, spatial intensity correlation and connectivity are used. The homogeneity of a space is normally defined as the cost function for traveling from a seed pixel to another location in the spatial domain based on a feature value.

Poon et al. [29] introduced the concept of region-based energy, where the homogeneity of a region is computed based on the intensity of a scalar image. For a vector image like that obtained with multispectral MRI (i.e., homogeneity, T1, T2, PD images), vector information from all the channels has been used for computing regional features. Figure 14 shows the results at different stages of snake deformation in delineation of the left ventricle from an MR image sequence using regional information. Other researchers [33–37] have also integrated region-based information into deformable contour models.

Region-based information is integrated along with the gradient into the snake model using a probabilistic approach [35]. A parametric curve is defined using a Fourier-based approach, where the idea is to use the number of harmonics depending on the required smoothness of the resulting contour. Thus, if the desired shape has more convexities, then higher Fourier harmonics are used, since the high frequency is encouraged by the geometry. Thus, the contour is expressed as

$$v(t) = \begin{pmatrix} x(t) \\ y(t) \end{pmatrix} = \begin{bmatrix} a_0 \\ c_0 \end{bmatrix} + \sum_{k=1}^{\infty} \begin{bmatrix} a_k & b_k \\ c_k & d_k \end{bmatrix} \begin{bmatrix} \cos(kt) \\ \sin(kt) \end{bmatrix}, \qquad (14)$$

where $v(t)$ is the contour and a_k, b_k, c_k, and d_k are the Fourier coefficients, with k ranging from 1 to ∞. The smoothness of the desired contour determines the number of harmonics to be used to define the geometry of the contour.

The contour can be deformed by changing the coefficients in the Fourier expression in Eq. (15). This is analogous to the internal energy of conventional snakes. The external features that guide the final destiny of the contour are defined

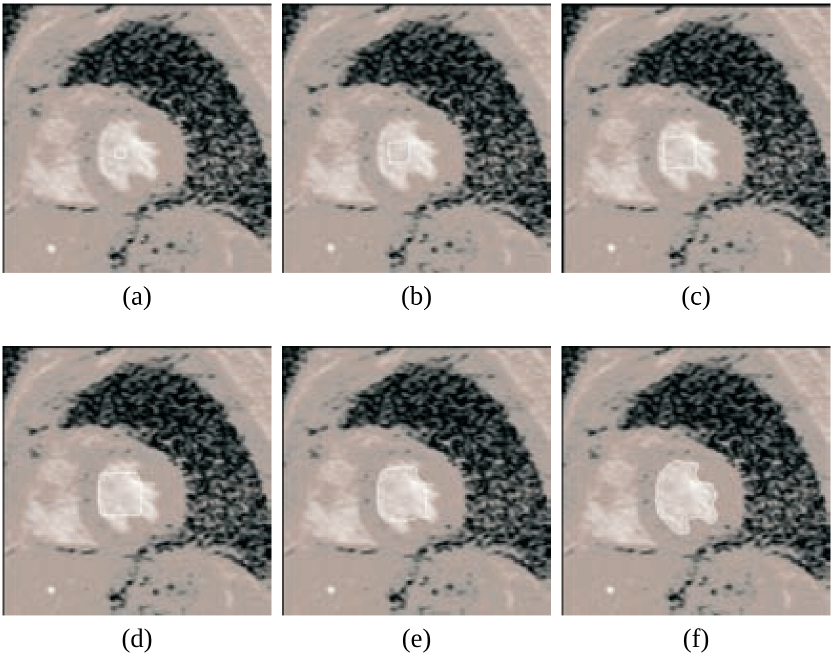

Figure 14. Evolution of region information-based snake for left ventricle segmentation from MR images. The homogeneity parameter is used in conjunction with the other standard energy functions, like geometric and edge functional, to evolve to the final contour, as shown by the white line in (g) from the initial contour in (a). See attached CD for color version.. Reprinted with permission from [29]. Copyright ©1997, Institute of Physics.

by maximizing the probability that the contour traverses through a high-gradient region and encloses a region having similar regional features. The regional feature can be defined in terms of the homogeneity of intensity or any other desired attribute. The intensity feature was used in the work reported by Chakraborty and colleagues [35], Thus, mathematically the work contour searches for minimizing the entropy or maximizing the likelihood function, defined by

$$\max_p\{P(p|\, I_g, I_s)\} = \max_p[\ln P(p) + \ln P(I_g\,|p) + \ln P(\ I_s\,|p)], \qquad (15)$$

where the first term on the right-hand side (RHS) defines the geometric shape parameter, and the second term is defined by the gradient along the contour. This term can be defined by computing the gradient, using the derivative of the Gaussian convolved with the intensity. The integral is taken over the entire curve. Thus, maximizing this function represents that for a given pattern of geometric shape the maximum possible need of the contour to cover the high-gradient region. In most medical images, due to the previously mentioned causes, the gradients in many

(a) (b) (c)

Figure 15. Illustration delineation of endocardium of heart using different methodologies: (a) manual segmentation by an expert; (b) semi-automated segmentation using only the gradient information into the deformable model; (c) same as (b) but with the regional information integrated along with geometric and gradient information. Reprinted with permission from [35]. Copyright ©1994, IEEE.

regions are very weak. Thus, with relaxation in geometric shape the contour tends to leak into other structures. Once the contour leaks, there is no force to stop this leakage, and return the contour to the desired structure. The regional features come to play in these regions of the image. The regional features are intended to prevent leakage through fuzzy and weak boundaries, since they use attributes other than simple local statistics. In a different form, these region-based approaches try to use global information derived in some form or other. The contour tries to maximize the homogeneous region enclosed by it. The region-based energy is thus defined as [35]

$$\ln P(I_s|\, p) = \iint\limits_A I_s(x,y)dA, \tag{16}$$

where $I_s(x,y)$ is the intensity at the pixel location (x,y) in the image, and the integral gives the total area A enclosed by the curve p.

The result of using regional information within a deformable model framework as described in Eqs. (12) and (13) is shown in Figure 15 for segmentation of the endocardium. As is evident, the region-based information visually improved the segmentation quality compared to the one using only gradient information.

The homogeneity feature has also been used for segmentation of an ultrasound image (see [32]). The external energy is defined using the homogeneity of the region through which a control point is moving. As the curve moves from one position to another while deforming, the position of the point also changes, and thus the associated intensity value (provided it is not moving through a homogeneous surface). Both the edge- and region-based energies have their own advantages and disadvantages. Edge-based energy can give good localization of the contour near the boundaries. Unfortunately, it has a small realm of attraction, thus requiring good initialization or a balloon force [13]. On the other hand, the region-based energy has a large realm of attraction and can converge even if explicit edges are not present. However, it does not as give good localization as the edge-based energy at image boundaries. The region-based energy defined in [32] attempts to ensure that in the region having maximum inhomogeneity the region-based force factor approaches zero to complement the gradient force. Also, the region-based energy is designed with the property that any control point will want to preserve the "nearness" to the initial intensity value from where it started. Thus, the defined force field has two factors — intensity difference from the initial location and local edge strength — and is equated as follows:

$$\gamma(\boldsymbol{\tau}(s_i^t)) = \left(1.0 - \left\|\psi(f(\boldsymbol{\tau}(s_i^t)) - \psi(f(\boldsymbol{\tau}(s_i^0))\right\|\right) * (1.0 - \psi\left(|\nabla G_\sigma \otimes f|\right)) . \tag{17}$$

In Eq. (18) the term $\left\|\psi(f(\boldsymbol{\tau}(s_i^t)) - \psi(f(\boldsymbol{\tau}(s_i^0))\right\|$ gives the difference of the normalized feature image between the points $\boldsymbol{\tau}(s_i^t)$ and $\boldsymbol{\tau}(s_i^0)$, where $\boldsymbol{\tau}(s_i^t)$ and $\boldsymbol{\tau}(s_i^0)$ represent the ith point on the contour at the tth and 0th iterations, respectively. f represents the feature image, which in this case is intensity. ψ represents a normalized feature. The first term in Eq. (18) tends to reduce the force, while the difference between the two feature values increases, i.e., tends to 1.0. On the other hand, the second term vanishes as the point approaches a high-gradient region. This force field thus tends to balance between the region-based homogeneity information and the local edge information [32]. Figure 16 illustrates the use of the above-mentioned region-based force field for segmenting ultrasound images. In both the cases the contour has been initiated outside the region of interest. It is to be noted that the active contour models that have been discussed so far are unidirectional in nature. Thus, they have the ability to either expand or contract depending on how they are set. Thus, the major challenge of this framework is that once the contour leaks through a boundary to the background, there is no force to bring it back to the object region. This limitation is due to the fact that the active contour does not have the knowledge of which region it belongs to. If this information can be imparted a priori to the snake process, then the deformation could be more controlled.

4. A-PRIORI INFORMATION

Use of factors like homogeneity provides better segmentation results compared to the local statistics-based approach; however, as discussed previously, they are limited by their inability to undertake bidirectional motion. The active contour model has unidirectional motion because of its lack of knowledge about object and background in any form of statistical information. If the snake can distinguish between object class and background class, then once it leaks from one structure to the other, the snake could go back to the desired interface. Thus, the active contour needs to be intelligent enough to distinguish between object

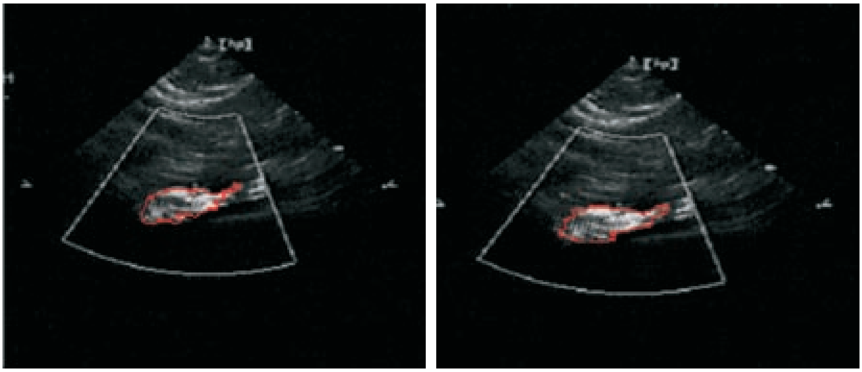

(a) (b)

Figure 16. Illustration of homogeneity-induced inertial snake [32] in segmentation of Doppler ultrasound images. See attached CD for color version.

and background. This can be accomplished if only some form of information that discriminates between object and background is known a priori.

4.1. Shape A Priori

Among other features, shape can be used to discriminate object from background. This is applicable where the target object has a well-defined shape, distinct from most other structures in the image. Some work has been reported using shape [38, 39] to identify object from background. If the shape pattern is known a priori from a set of statistical distributions of object shapes, then a shape model can be defined based on those available shapes. These shape models are usually defined as probabilistic distributions, where a Gaussian distribution is defined for each of the “modes” of the shape about a mean model. This “mode” can be represented in any form, like a Fourier [38] or point-wise representation [40, 41], or some other form of expression. In each case, the underlying theory is to define a symmetric model that captures the statistical variation of the a-priori shapes from a mean shape defined as

$$\bar{\mathbf{x}} = \frac{1}{N}\sum_{i=0}^{N-1}\mathbf{x}_i, \tag{18}$$

where $\bar{\mathbf{x}}$ is the mean shape, and $\mathbf{x}_i$ is the ith shape vector defined by some form of shape descriptor. N is the total number of shapes known a priori. The main motivation is to represent a curve in using a shape descriptor and associate a probability distribution on the parameters based a-priori knowledge about the shape. The prior information available is a flexible bias toward more likely shapes. The parameterization itself should be expressive enough to represent any potential shape of a given geometric type, and the associated probability distribution will introduce a bias toward an expected range of shapes. The spread in distributions is due to the variability among instances of the object. If a particular distribution is known to govern the parameters, it can be used as prior probability. On the other hand, if the mean and standard deviation of the distribution is known, an independent multivariate Gaussian can be used for all parameters:

$$P(\mathbf{p}) = \prod_{i=0}^{N} P(p_i) = \prod_{i=0}^{N} \frac{1}{\sigma_i \sqrt{2\pi}} e^{-\frac{(p_i - m_i)^2}{2\sigma_i}}, \tag{19}$$

where N is the number of parameters, p_i is the ith parameter value, and m_i and σ_i are the mean and standard deviation.

It is important to mention at this stage that a Gaussian distribution has certain beautiful properties that make it the choice for most probabilistic distributions. Among the probability densities with a given variance, the Gaussian is the one with maximum entropy [38]. Moreover, the Gaussian is a symmetric distribution about its mean. Thus, the Gaussian density follows directly from knowing no information other than mean and variance. Since for most of the distribution any bias is not desirable, the Gaussian distribution is the most effective choice in approximating a probability density function.

Once the probabilistic model has been designed, to apply this a-priori knowledge to the problem of boundary determination, a maximum a-posteriori criterion has been formulated. Let $I(x, y)$ be the image data and $t_{\mathbf{p}}(x, y)$ an image template corresponding to a particular value of the parameter vector. In terms of probability, to decide which template $t_{\mathbf{p}}$ and image I correspond with the probability of the template, given the image given by $P(t_{\mathbf{p}}|I)$, the maximum over $\mathbf{p}$ needs to be determined, which can be mathematically expressed as [38]

$$P(t_{\max}|I) = \max_{\mathbf{p}} P(t_{\mathbf{p}}|I) = \max_{\mathbf{p}} \frac{P(t_{\mathbf{p}}|I)P(t_{\mathbf{p}})}{P(I)}. \tag{20}$$

Maximizing a-posteriori probability gives the desired template fit in an image. Figure 17 illustrates segmentation of synthetic images using a-priori shape information within the deformable model framework.

4.1.1. Application and Discussion

Shape a priori was used within the snake framework for detection of brain cortex in [39]. A cross-section of brain cortex is modeled as a ribbon, and a constant speed mapping of its spine is sought. A variational formulation and associated force balance conditions are used for convergence of the snake. The model uses only elastic forces, and the curvature term is dropped from the force balance equation. The external force is tailored for application into structures like

(a) (b) (c)

Figure 17. Illustration of using shape-based prior in the deformable model framework: (a) shape priors with the mean shape and with a standard deviation around one parameter; (b,c) results of [38] on synthetic images. Reprinted with permission from [38]. Copyright ©1992, IEEE.

the cortex, which has a nearly constant width throughout its extent. The force field is defined such that if a small disk centered at a point on the active contour rests entirely within the ribbon, it experiences no external force; if, on the other hand, a portion of the disk intersects adjacent tissue, the disk experiences a force drawing it back toward the cortex.

These approaches showed some promise in the particular cases where the shape distributions are known a priori or the solution was tailored for the specific application and shape [39]. However, the main limitations of incorporating this information into the active contour model is a loss of its generality and deformability within a geometric paradigm, which is probably the most attractive feature of an active contour model. Unifying the a-priori shape information with image data in an active contour model has been proposed by many researchers [42–46]. A separate class of compact representations of shape and image data within the deformable model framework inspired the active shape model [40] and the active appearance model [41].

4.2. Feature Space

The purpose of incorporating a-priori features is principally to balance the force equation in such a way that the contour will converge from both the object and background toward the interface. To strike this balance it is required to optimally use information about object and background so that the regional features will drive the snake from any image location toward the object–background interface. Therefore, the image surface needs to be defined in such a manner that when the contour lies within object class (defined in some form), the force field acts in such a way that the energy minimization criteria are reached if and only if the contour expands to propagate toward the interface. On the other hand, if a contour point

(a) (b)

Figure 18. Illustration of the result of dual active contour model (a) initialization of the two contours (shown in white); (b) result after convergence. Reprinted with permission from [47]. Copyright ©1997, IEEE.

lies in the background region, it should experience a contracting force. In this particular situation, it is assumed that the object is entirely contained within the background. Figure 18 illustrates some results using the dual active contour model, where two contours attempt to integrate the information from a contour expanding within a feature to a contour contracting from outside the feature [47]. Though conceptually this is something the a-priori information is designed to accomplish, this method in principle does not use any explicit form of prior statistical image information to drive the snake. Object feature information can be used analogous to how shape information has been incorporated within the snake framework. The idea is to define the statistical distribution of the feature space from prior-known segmented object–background data and define a regional force field using this information.

The statistical snake proposed by Ivins and Porill [31] addressed this feature by incorporating an energy term that generates a bidirectional pressure force depending on a-priori information of the image data. A regional feature defines the modified external energy over the area as follows:

$$E_{\text{region}} = -\iint_R G(f(x,y))dxdy, \tag{21}$$

where G is the function that measures the nature of the image data. For a unidirectional snake with a balloon or like forces the value of $G(f(x,y))$ is set to +1 or –1 depending on whether the snake is expanding or contracting. In a statistical snake, this measure will change the direction depending on the nature of $f(x,y)$

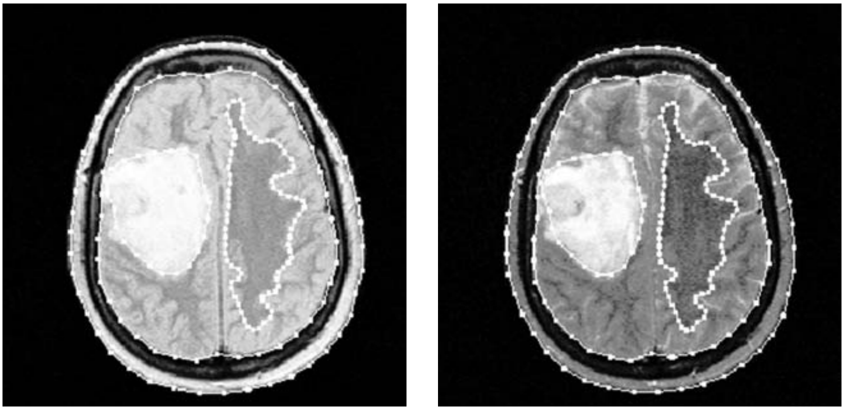

(a) (b)

Figure 19. Segmentation results in sections of NMR images of brain using statistical snake. Reprinted with permission from [31]. Copyright ©1994, British Machine Vision Association Press.

and is defined as

$$G(f(x,y) = \begin{cases} +1 & \text{if } |f(x,y) - \mu| \leq k\sigma, \\ -1 & \text{if } |f(x,y) - \mu| > k\sigma, \end{cases} \tag{22}$$

where μ defines the mean, and σ is the standard deviation of the intensity distribution in the object region. Thus, the force field exerts a unit outward pressure when the contour is inside the object region and an inward pressure when the contour lies outside the object region. This is attributable to the bidirectional nature of the active contour model. The force can be modeled to vary with the distance from the mean of the object intensity, i.e., when the control point of the snake is near a mean object feature, the propagation force is high, and as it moves away from the mean the force decreases, until it starts reversing direction as it crosses the entire object feature distribution zone. A linear model and a model based on Mahalanobis distance are also computed in [31].

These approaches are essentially a probabilistic approach with a pixel having a certain confidence level belonging to some a-priori distribution. Suppose the image has two main regions, with different probability distributions. A simple example is the case where we have to segment a white object from a dark background; the regions will have different means and possibly different variances. Jacob et al. [48] used a region likelihood function defined as follows:

$$E_{\text{region}} = -\int_S \log(P(f(s)|s \in R_1))ds - \int_{S'} \log\ P(f(s)|s \in R_2))ds, \tag{23}$$

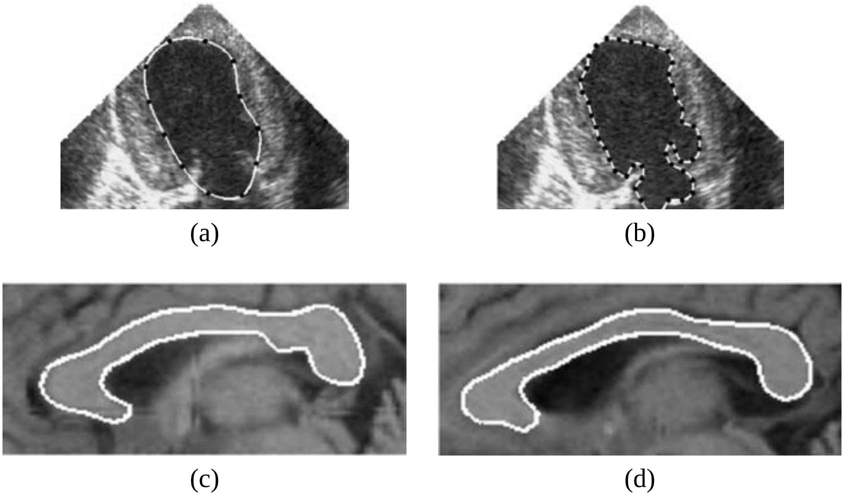

Figure 20. Segmentation results using the probabilistic model proposed in [48]: (a) initial contour drawn on an ultrasound image of dog heart; (b) final segmentation result; (c,d) segmentation of corpus callosum from MR images. Reprinted with permission from [48]. Copyright ©2004, IEEE.

where R_1 and R_2 are two regions in the image and the entire image domain $R = R_1 \cup R_2$. S and S' are the regions inside and outside the curve, respectively. Thus, the optimal segmentation is obtained when $S = R_1$ and $S = R_2$. It can be shown that Eq. (23) can be rewritten as [48]

$$E_{\text{region}} = \int_S - \left(\frac{\log(P(f(s)|s \in R_1))}{\log(P(f(s)|s \in R_2))} \right) ds. \tag{24}$$

Figure 20 illustrates segmentation results using the probabilistic model in [48]. Evaluation of the energy minimization equation for the snake using this kind of probability density function requires estimation of these functions. As previously mentioned, the probability is estimated from the a-priori information and approximated as a Gaussian distribution with a certain mean and standard deviation. In situations where the a-priori distributions are not known, they can be estimated dynamically [48]. However, there is risk involved with this dynamic approach of incorporating more uncertainty into the system. Nevertheless, the probabilistic approach has proved to be a better solution for snake decomposition compared to the one without any a-priori information. It is important to note that Eqs. (24) and (25) balance the force from both the object and background feature space in contrast to Eq. (23), which uses information about only the object feature. Since by principle the requirement is to optimally use the information from the two regions, so it is recommended that both feature spaces be used for definition of the force equation.

Many other investigators have used the a-priori Gaussian distribution model (see, e.g., [24, 49–51]). With all these approaches, the main intention is to capture the confidence level of a pixel belonging to some region. Das et al. [24] developed an active contour model using the a-priori information within a class uncertainty [52] framework.

Given a priori knowledge of object/background intensity probability distributions, the object/background class of any location can be determined based on its intensity value and establish the confidence level of the classification [52]. The pixels with a higher confidence of belonging to the object class exert a high expanding force on the contour, while those with a high confidence of belonging to the background generate a high contracting force. It can be conjectured that the pixels near the object–background interface will have the lowest confidence of belonging to either of the classes and will represent the region of highest uncertainty. This is based on the assumption that there is a certain amount of mixing between the two intensities at the interface, which is true for most practical images due to effects like blurring, partial voluming effect, etc.

Given the probabilities for any pixel with intensity f belonging to object and background as $p_O(f)$ and $p_B(f)$, respectively, and $p(f)$ being the total probability given by $p(f) = p_O(f) + p_B(f)$, the class uncertainty of a pixel with intensity f is expressed as

$$h(f) = -\frac{p_O(f)}{2p(f)} \log \frac{p_O(f)}{2p(f)} - \frac{p_B(f)}{2p(f)} \log \frac{p_B(f)}{2p(f)}. \tag{25}$$

The class uncertainty is highest at the object–background interface, where the pixel intensities are in the most un-deterministic state. The force field is defined as follows:

$$\mathbf{F}_{\text{region}}(\boldsymbol{\tau}(s_i)) = \begin{cases} 1 - h(f(\boldsymbol{\tau}(s_i)) & \text{if } f(\boldsymbol{\tau}(s_i) \in \text{object}, \\ -(1 - h(f(\boldsymbol{\tau}(s_i))) & \text{if } f(\boldsymbol{\tau}(s_i) \in \text{ background.} \end{cases} \tag{26}$$

Thus, the force field will assist faster movement of the contour in the homogeneous region and will slow down as it approaches the boundary. Other conventional force fields have been used with this contour model [49]. The performance of a class uncertainty-induced snake on medical phantoms and MR images of carotid artery is depicted in Figure 21.

Other deformable model classes like the level sets also use a-priori classification information. Many significant works have been published using this technique [53–57]. However, active shape models and level sets are not within the purview of this chapter, and so interested readers are encouraged to refer to the above-mentioned references.

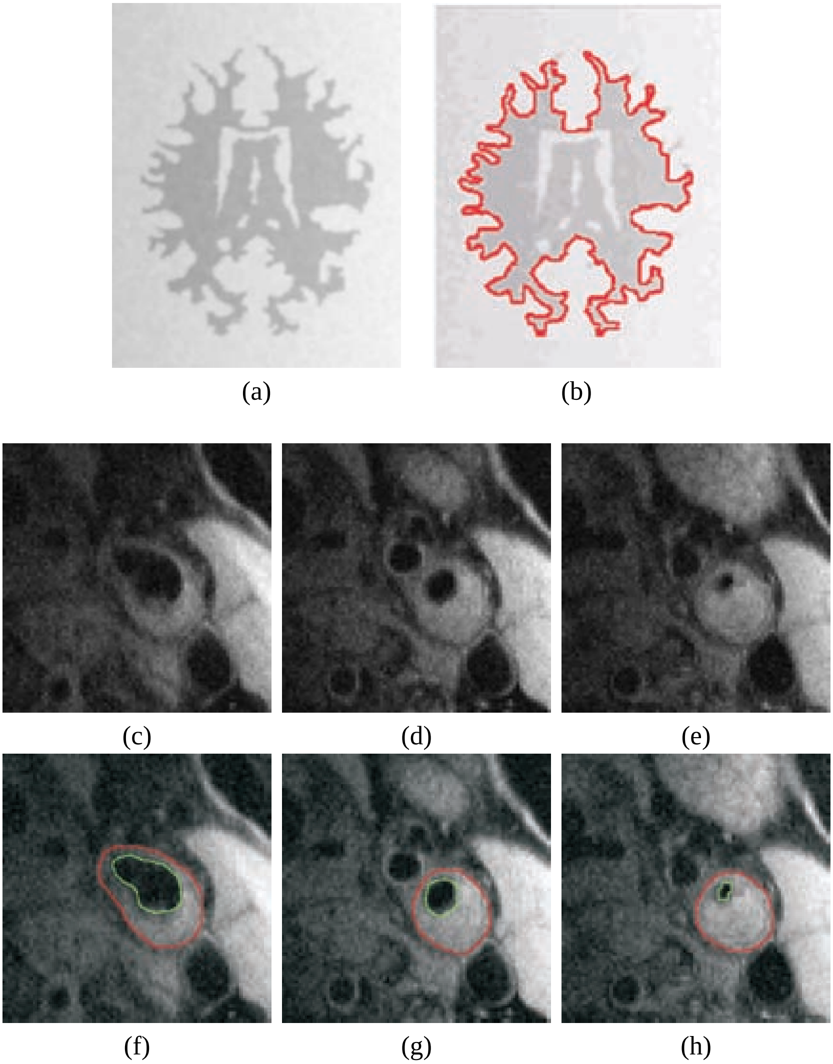

Figure 21. Illustration of class uncertainty-induced snake: (a) phantom image generated from segmented mask of brain with noise and inhomogeneity added; (b) segmentation using class uncertainty-induced active contour [49]; (c–e) cropped region showing carotid artery in MR images (courtesy Hospital of the University of Pennsylvania); (f–h) segmentation of lumen (green) and outer vessel wall (red) using the class uncertainty based snake. See attached CD for color version.

One of the major advantages of the level set approach is its adaptability to topological changes. Traditional snakes, on the other hand, are restricted by their inability to respond to topological variations. The topology of the structure of interest must be known a priori since traditional snakes models being parametric representations are incapable of topological transformations without additional intervention. Samadani [58] used a heuristic technique based on deformation energies to split and merge active contours. More recently, Malladi et al. [54] and Caselles et al. [51] independently developed a topology-independent active contour scheme based on the modeling of propagating fronts with curvature-dependent speeds, where the propagating front is viewed as an evolving level set of some implicitly defined function.

5. TOPOLOGICAL SNAKE

Topological adaptivity requires the multiple instances of the model to be dynamically created or destroyed, or can seamlessly split or merge as the object to be segmented changes its topology. Much research has been dedicated to this area [59–61]. The main principle behind each of these approaches involves using the grid information to establish a relation between the parametric curve and the pixel domain. Conversion to and from the traditional snakes model formulation requires the ability to discard or impose the grid within the framework at any time. The grid needs to provide a simple and effective means to extend the geometric and topological adaptability of snakes. McInerney and Terzopoulos [59] developed a parametric snakes model that has the power of an implicit formulation by using a superposed simplicial grid to reparameterize the model during the deformation process. Of all the approaches, we will detail this approach since it is the one most widely used. As previously mentioned, the idea is to incorporate the traditional snakes model within the framework of simplicial domain decomposition.

The grid of discrete cells used to approximate the snake model is an example of space partitioning by simplicial decomposition. There are two main types of domain decomposition methods: non-simplicial and simplicial. Most non-simplicial methods employ a regular tessellation of space. The marching cubes algorithm is an example of this type of method. These methods are fast and easy to implement, but they cannot be used to represent surfaces or contours unambiguously without the use of a disambiguation scheme.

Simplicial methods, on the other hand, are theoretically sound because they rely on classical results from algebraic topology. In simplicial decomposition, space is partitioned into cells defined by open simplices, where an n-simplex is the simplest geometrical object of dimension n. A simplicial cell decomposition is also called a *triangulation*.

The simplest triangulation of Euclidean space R^n is a Coxeter-Freudenthal triangulation (Figure 22a). It is constructed by subdividing space using a uniform cubic grid, and the triangulation is obtained by subdividing each cube into $n!$ simplices. Simplicial decompositions provide an unambiguous framework for

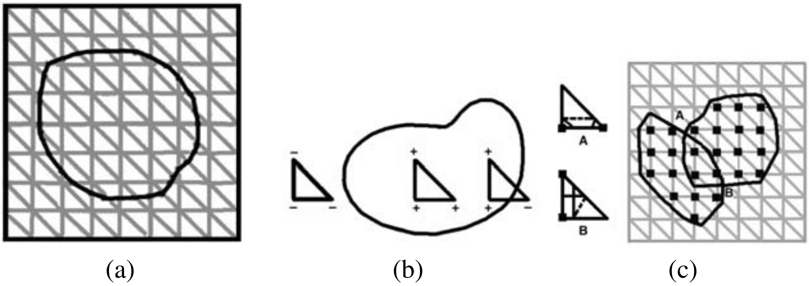

Figure 22. (a) Simplicial approximation of contour model using a Freudenthal triangulation [59]. (b) Cell classification. (c) Intersection of two snakes with "inside" grid cell vertices marked. Snake nodes in triangles A and B are reconnected. Reprinted with permission from [59]. Copyright ©1995, IEEE.

the creation of local polygonal approximations of a contour or surface model. In an n-simplex, the negative vertices can always be separated from the positive vertices by a single plane; thus, an unambiguous polygonalization of the simplex always exists, and as long as neighboring cubes are decomposed so that they share common edges (or faces in 3D) at their boundaries, a consistent polygonization will result. The set of simplices (or triangles in 2D) of the grid that intersect the surface or contour (the boundary triangles) form a two-dimensional combinatorial manifold that has as its dual a one-dimensional manifold that approximates the contour. The one-dimensional manifold is constructed from the intersection of the true contour with the edges of each boundary triangle, resulting in one line segment that approximates the contour inside this triangle (Figure 22a). The contour intersects each triangle in two distinct points, each located on a different edge. The set of all these line segments constitutes the combinatorial manifold that approximates the true contour.

The cells of the triangulation can be classified in relation to the partitioning of space by a closed contour model by testing the "sign" of the cell vertices during each time step. If the signs are the same for all vertices, the cell must be totally inside or outside the contour. If the signs are different, the cell must intersect the contour (Figure 22b).

The simplicial decomposition of the image domain also provides a framework for efficient boundary traversal or contour tracing. This property is useful when models intersect and topological changes must take place. Each node stores the edge and cell number it intersects, and, in a complementary fashion, each boundary cell keeps track of the two nodes that form the line segment cutting the cell. Any node of the model can be picked at random to determine its associated edge and cell number. The model can then be traced by following the neighboring cells indicated by the edge number of the connected nodes.

When a snake collides with itself or with another snake, or when a snake breaks into two or more parts, a topological transformation must take place. In order to effect consistent topological changes, consistent decisions must be made about disconnecting and reconnecting snake nodes. The simplicial grid provides us with an unambiguous framework from which to make these decisions. Each boundary triangle can contain only one line segment to approximate a closed snake in that triangle. This line segment must intersect the triangle on two distinct edges. Furthermore, each vertex of a boundary triangle can be unambiguously classified as inside or outside the snake. When a snake collides with itself, or when two or more snakes collide, there are some boundary triangles that will contain two or more line segments. We then choose two line segment endpoints on different edges of these boundary triangles and connect them to form a new line segment. The two endpoints are chosen such that they are the closest endpoints to the outside vertices of the triangle and such that the line segment joining them separates the inside and outside vertices (Figure 22c). Any unused node points are discarded.

Once the topological transformations have taken place, the list of nodes generated can be visited and contour tracings perform via the grid cells, marking off all nodes visited during the tracings. All new snakes generated are determined by the topological transformation phase and assign each a unique identifier.

Topological adaptive snakes are widely used [59, 60, 63] for their ability to handle complex structures which are so often encountered in medical imaging. Figure 23 illustrates some of the implementation results for tracking blood vessels in a retinal angiogram, on the cerebral vasculature surface (3D), and in different regions of brain. It is important to notice that topological adaptability has allowed an immense amount of flexibility in the snake framework, and thus enabled it to segment geometrically and topologically complex structures.

6. DISCUSSION AND CONCLUSIONS

The basic snake algorithm thus developed originally for computer vision applications has found widespread application in medical image analysis for its ability to capture local image statistics within a global geometric framework. This framework is widely appreciated in segmenting anatomical structures and quantifying various features in images of different modalities, including MR, x-ray, CT, and ultrasound. The task of segmentation using an active contour model ranges throughout the anatomical atlas, covering areas, like spine, heart, brain, cerebrum, kidney, lungs, and liver, and various artery segmentation, like the carotid and the aorta. An extensive amount of work has been done in delineating and quantifying the growth of objects like tumors, multiple sclerosis lesions, a fetus, micro-calcifications in breast from mammography images, etc. Thus, applications range from identifying white matter in the brain to quantifying diseases through imaging. Also, application of the active contour model has gone a step further in

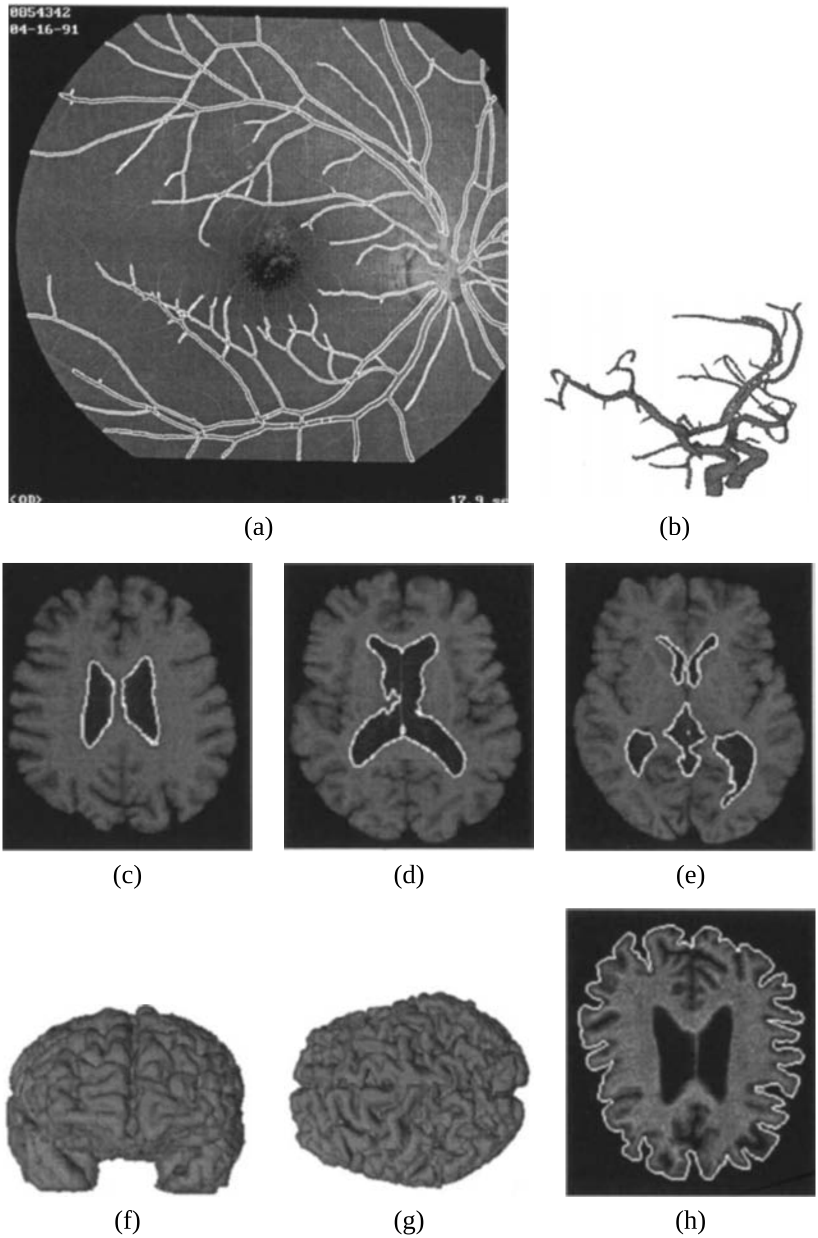

Figure 23. Illustration of results of segmentation using topology-adaptive active contour model on 2D images and 3D volumes [60]. (a) Segmentation of blood vessels in retinal angiography. T-surface segmentation of (b) cerebral vasculature from MR image volume; (c–e) ventricles from MR image volume of the brain; (f–h) different view of cerebral cortex segmentation using T-surface. Reprinted with permission from [60]. Copyright ©1999, IEEE.

identifying cellular structures and cell motion. This wide range of applications essentially covers both the 2D and 3D image domain for signifying both volume and temporal data. Motion tracking using 3D temporal data has also been widely studied for cardiac, pulmonary, and arterial motion in 4D MR, CT, etc., and even to the level of cellular motion from molecular imaging devices. At the present time, the deformable model-based segmentation algorithm has become a vital part of the most advanced image processing toolbox associated with medical imaging devices.

Most clinical applications presently use manual segmentation of the region of interest, that is, a domain expert goes through each of the image slices over the entire volume, or temporal data, and manually identifies and delineates the region of interest by using a mouse-guided framework. This has several disadvantages: the manual segmentation process is extremely tedious and time consuming. Furthermore, the image segmentation is nonreproducible and prone to operator bias. Thus, computer-assisted methodologies with minimal user intervention need to replace the manual segmentation process to obtain accurately reproducible segmentation.

This chapter has attempted to focus on the development of the active contour model to meet the various requirements in medical image segmentation and analysis. Segmentation of medical images is required for accurate and reproducible analysis of data for a huge range of applications, including diagnosis, postoperative study, and interactive surgical procedures. Manual segmentation is the most common technique used by physicians to process data. However, with the amount of data exploding and due to the nonreproducibility of the results, there is an inherent need for automated or semi-automated computerized algorithms that can generate segmentation results accurately and reproducibly. Segmentation processes that use low-level image processing have not been sufficient to segment complex structures from images and provide an accurate continuous boundary due to their dependence on local statistics, which in turn are corrupted by noise and other artifacts. The deformable model has been found to be quite efficient in this context, since it uses physics-based constraints along with local image statistics in a very natural way. The initial design of the active contour itself generated a lot of interest. With the complexity of the task increasing, the requirements are becoming more demanding, and subsequent improvements have followed. Efforts are being made to make the deformation less sensitive to initialization [13, 26]. Dependence on the gradient force alone for growth and termination of the active contour forces the snake to fail in images with weak and fuzzy boundaries, since the edge functional is not well defined in those regions. Regional information, like homogeneity and contrast, improved the active contour model. The snake evolution using regional information and local statistics, like gradient, captured the object effectively as the propagation was controlled by the regional force rather than a blind force. A-priori information even made the snake bidirectional, thus helping it to prevent leakage. Performance was thus enhanced with incorporation of this form of energy. Another major advancement of the active contour model came in the form of inclusion of topological adaptability, where the snake can merge and split to capture complex geometries and topologies.

The equations in this chapter mostly deal with a 2D space. However, they are extendable to 3D in all cases [25, 60]. The basic energy equation remains the same for all dimensionalities. Only the computation of geometric properties and image forces is changed. The geometric properties then need to be evaluated for a surface rather than a line segment. This makes the estimation computationally expensive, but the main essence is retained. The snake framework can be utilized in a different form often to segment 3D volumes. Rather than using the surface, the 3D volume can be broken down into an array of 2D slices (which comes naturally in medical images). Each of the 2D slices can be separately segmented and stacked up to form a 3D volume. However, in this approach the 3D information of the medical data is not utilized optimally.

A similar approach has also been used for motion tracking in various medical applications like tracking heart motion [64] and cell deformation [28, 65–69]. Deformable models have been used to track nonrigid microscopic and macroscopic structures in motion, such as blood cells [65] and neurite growth cones [70] in cine-microscopy, as well as coronary arteries in cine-angiography [71]. However, the primary use of deformable models for tracking in medical image analysis is to measure the dynamic behavior of the human heart, especially the left ventricle. Regional characterization of heart wall motion is necessary to isolate the severity and extent of diseases such as ischemia. The most conventional approach is to track the 2D contour in an image frame and propagate the contour to the temporally next frame for deformation. Some approaches have utilized motion vectors and Kalman filtering approaches [66] to boost snake performance in tracking motions of this kind.

The increasingly important role of medical imaging in the diagnosis and treatment of disease and the rapid advancement in imaging devices have opened up challenging problems for the medical image analysis community. Deformable models offer an attractive solution to situations where we intend to capture complex shapes and wide shape variability of anatomical structures. Deformable models overcome many of the limitations of traditional low-level image processing techniques by providing compact and analytical representations of object shape, by incorporating anatomic knowledge, and by providing interactive capabilities.

APPENDIX A

Energy minimization of the snake is accomplished within an Euler-Lagrangian framework of solving PDEs or a dynamic programming approach that uses neighborhood information on an energy surface. Note that the energy-based approach of dynamic programming and the greedy snake does not optimally use the image vector information. Pseudocode for the PDE-based and the greedy snake methods are provided in this appendix:

A. Pseudocode for Snake Computation Using the PDE Approach

1. **Input image** $I(x,y)$
2. **Preprocessing**
   (a) **Compute feature map (Input Image I)**
      i. **Compute gradient map G = $\nabla G_\sigma \oplus$ I**
         A. **Normalize G**
      ii. **Compute regional information-based normalized feature map F**
3. **Input discrete points**
4. **Define a contour through the sample points on the curve**
5. **Input parameter values for snake computation:** α = strength of elasticity; β = rigidity strength; γ = gradient strength; η = other factor **(might be regional or user-defined constraints). The number of parameters introduced will be equal to the number of force fields used.**
6. **Define stiffness matrix**

$$K = \begin{bmatrix} c_1 & b_1 & a_1 & \dots & \dots & \dots & \dots & \dots & a_{N-1} & b_N \\ b_1 & c_2 & b_2 & a_2 & \dots & \dots & \dots & \dots & 0 & a_N \\ a_1 & b_2 & c_3 & b_3 & a_3 & \dots & \dots & \dots & 0 & 0 \\ 0 & a_2 & b_3 & c_4 & b_4 & a_4 & \dots & \dots & \dots & \dots \\ \dots & \dots & \dots & \dots & \dots & \dots & \dots & \dots & \dots & \dots \\ \dots & \dots & \dots & \dots & \dots & \dots & \dots & \dots & \dots & \dots \\ \dots & \dots & \dots & \dots & \dots & \dots & \dots & \dots & \dots & \dots \\ 0 & 0 & \dots & \dots & \dots & a_{N-4} & b_{N-3} & c_{N-2} & b_{N-2} & a_{N-2} \\ a_{N-1} & 0 & \dots & \dots & \dots & 0 & a_{N-3} & b_{N-2} & c_{N-1} & b_{N-1} \\ b_N & a_N & \dots & \dots & \dots & 0 & 0 & a_{N-2} & b_{N-1} & c_N \end{bmatrix},$$

$$h^4 a_i = \beta_{i+1},$$
$$h^4 b_i = -2\beta_i - 2\beta_{i+1} - h^2\alpha_{i+1},$$
$$h^4 c_i = \beta_{i-1} + 4\beta_i + \beta_{i+1} + h^2\alpha_i + h^2\alpha_{i+1},$$

where α, β are the coefficient values.

1. **While (Iterations $\neq$ Maximum Iterations)**

(a) **Construct the coordinate matrix:** $\mathbf{X} = \{$x(0), x(1), x(2),.....,x(N-1)$\}^T$
$\mathbf{Y} = \{$y(0), y(1), y(2),.....,y(N-1)$\}^T$

(b) **Construct matrix from external energy and information:** $\mathrm{B}_x(\bullet, t-\Delta t, t-2\Delta t), \mathrm{B}_y(\bullet, t-\Delta t, t-2\Delta t)$**, where** B_x **denotes the** x**-derivative values of the external energy** $\left(\frac{\partial}{\partial x}E_{\text{ext}}\right)$ **and** $\mathrm{B}_y = \frac{\partial}{\partial y}E_{\text{ext}}$**.** t **represents the iteration index with separation** Δt=1 **for most cases.**

(c) **Solve** $\mathbf{X} = \mathbf{K}^{-1}\mathbf{B}_x$ **and** $\mathbf{Y} = \mathbf{K}^{-1}\mathbf{B}_y$

(d) **iterations++**

(e) **ReSample Curve**

2. **End and fit spline to the final contour.**

B. Pseudocode for Snake Computation Using Local Neighborhood Energy-Based Approach

1. **Input image** $I(x, y)$

2. **Preprocessing**

   (a) **Compute feature map (Input Image** I**)**

   i. **Compute gradient map G =** $\nabla G_\sigma \oplus$ **I**

   A. **Normalize G**

   ii. **Compute regional information-based normalized feature map F**

3. **Input discrete points**

4. **Define a contour through the sample points on the curve**

5. **Input parameter values for snake computation:** α = strength of elasticity; β = rigidity strength; γ = gradient strength; η = other factor **(might be regional or user-defined constraints). The number of parameters introduced will be equal to the number of force fields used.**

6. **While (Iterations != Maximum Iterations)**

   (a) **For (i=0; i<N; i++) /* N = Number Of Control Points */**

   i. **Search the** 3×3 **neighborhood (for 2D)**

   A. **Compute Energy due to all the factors at each neighborhood**

   B. **Find the lowest energy neighborhood pixel**

   C. **Assign the point to this lowest energy neighborhood**

ii. **Update the contour information**

(b) **Iterations++;**

7. **End and fit spline to the final contour.**

Note that in both cases it important to ensure that any movement of the contour that violates the topological circle configuration of the curve is avoided, that is, there cannot be any self-intersecting lines in the contour.

APPENDIX B

Incorporation of a priori information in the form of some probabilistic approach is detailed in this appendix. Specifically, the pseudocode for defining intensity-based object background confidence classification is provided.

Pseudocode for Object–Background Classification Based on Intensity

1. **Input Image** $I(x, y)$
2. **Input object distribution information (object mean, object std deviation)**
3. **Input background intensity distribution (background mean, background std. deviation)**
4. **Construct One-Sided Gaussian Probability Density Function:**
   (a) **If (Object mean $>$ Background mean)**
      i. **For (intensity = Minimum Intensity; intensity $<$ =Maximum Intensity, intensity++)**
         A. **if (intensity $<$ =Object Mean)**
         B. **Object Probability (intensity) = exp(–(intensity – Object Mean)^2/(2*(Object Std Deviation)^2);**
         C. **else**
         D. **Object Probability (intensity) = 1.0;**
         E. **if (intensity$<$=background mean)**
         F. **Background Probability (intensity) =1.0;**
         G. **else**
         H. **Background Probability (intensity) = exp(–(intensity – Background Mean)^2/(2*(Background Std Deviation)^2);**

   (b) **else**
      i. **For (intensity = Minimum Intensity; intensity $<$ =Maximum Intensity, intensity++)**

A. **if (intensity < = Object Mean)**
B. **Object Probability (intensity) = exp(–(intensity – Object Mean)^2/(2*(Object Std Deviation)^2);**
C. **else**
D. **Object Probability (intensity) = 1.0;**
E. **if((intensity<=background mean)**
F. **Background Probability (intensity) =1 .0;**
G. **else**
H. **Background Probability (intensity) = exp(–(intensity – Background Mean)^2/(2*(Background Std Deviation)^2);**

(c) **For the entire image compute the probability map at each pixel.**

7. REFERENCES

1. Haacke EM, Brown RW, Thompson MR, Venkatesan R. 1999. *Magnetic resonance imaging: physical principles and sequence design*. New York: Wiley-Liss.
2. Kurut EK, McIlwain EF, Plotnick GD. 2004. *Handbook of echo-doppler doppler interpretation*, 2d ed. Boston: Blackwell Futura.
3. Calender WA. 2000. *Computed tomography: fundamentals, system technology, image quality, applications*. Weinheim: Wiley-VCH.
4. Wahl RL. 2002. *Principles and practice of positron emission tomography*. Philadelphia: Lippincott Williams & Wilkins.
5. Huettel SA, Song AW, McCarthy MC. 2004. *Functional magnetic resonance imaging*. Sunderland, MA: Sinauer Associates.
6. Wernick MN, Aarsvold JN. 2004. *Emission tomography: the fundamentals of PET and SPECT*. New York: Academic Press.
7. Fischler M, Elschlager R. 1973. The representation and matching of pictorial structures. *IEEE Trans Comput* **22**(1):67–92.
8. Widrow B. 1973. The rubber mask technique, part I. *Pattern Recognit* **5**(3):175–211.
9. Terzopoulos D. 1986. Regularization of inverse visual problems involving discontinuities. *IEEE Trans Pattern Anal Machine Intell* **8**(4):413–424.
10. Kass M, Witkin A, Terzopoulos D. 1988. Snakes: active contour models. *Int J Comput Vision* **1**:321–331.
11. Terzopoulos D, Fleischer K. 1988. Deformable models. *Visual Comput* **4**(6):306–331.
12. McInerney T, Terzopoulos D. 1996. Deformable models in medical image analysis: a survey. *Med Image Anal* **1**(2):91–108.
13. Cohen LD, Cohen I. 1993. Finite-element methods for active contour models and balloons for 2-d and 3-d images. *IEEE Trans Pattern Anal Machine Intell* **15**(11):1131–1147.
14. Amini AA, Weymouth TE, Jain RC. 1990. Using Dynamic programming for solving variational problems in vision. *IEEE Trans Pattern Anal Machine Intell* **12**:855–867.
15. Williams DJ, Shah MA. 1992. Fast algorithm for active contours and curvature estimation. *Comput Vision Graphics Image Process: Image Understand* **55**:14–26.
16. Carlbom I, Terzopoulos D, Harris K. 1994. Computer-assisted registration, segmentation, and 3D reconstruction from images of neuronal tissue sections. *IEEE Trans Med Imaging* **13**(2):351–362.

17. Cohen I, Cohen LD, Ayache N. 1992. Using deformable surfaces to segment 3D images and infer differential structures. *Comput Vision Graphics Image Process: Image Understand* **56**(2):242–263.
18. Berger M-O, Mohr R. 1990. Towards autonomy in active contour models. In *Proceedings of the 19th international conference on pattern recognition,* Vol. 1, pp. 847–857. Washington, DC: IEEE.
19. Leymarie F, Levine MD. 1992. Simulating the grassfire transform using an active contour model. *IEEE Trans Pattern Anal Machine Intell* **14**:56–75.
20. Lobregt S, Viergever MA. 1995. A discrete dynamic contour model. *IEEE Trans Med Imaging* **14**:12–24.
21. Falcao AX, Udupa JK, Samarasekera S, Hirsch BE. 1996. User-steered image boundary segmentation. *Proc SPIE* **2710**:278–288.
22. Falcao A, Udupa JK. 1997. Segmentation of 3D objects using live wire. *Proc SPIE* **3034**:228–235.
23. Park HW, Schoepflin T, Kim Y. 2001. Active contour model with gradient directional information: directional snake. *IEEE Trans Circ Syst Video Technol* **11**:252–256.
24. Das B, Saha PK, Wehrli FW. 2004. Object class uncertainty induced snake with application to medical image segmentation. *Proc SPIE* **5370**:369–380.
25. Xu C, Prince J. 1998. Snakes, shapes, and gradient vector flow. *IEEE Trans Image Process* **7**:359–369.
26. Das B, Banerjee S. 2004. Inertial snake for contour detection in ultrasonography images. *IEEE Proc Image Signal Process* **151**:235–240.
27. Paragios N, Deriche R. 2000. Geodesic active contours and level sets for the detection and tracking of moving objects. *IEEE Trans Pattern Anal Machine Intell* **22**:266–280.
28. Ma T, Tagare HD. 1999. Consistency and stability of active contours with euclidean and non-Euclidean arc lengths. *IEEE Trans Image Process* **8**:1549–1560.
29. Poon CS, Braun M. 1997. Image segmentation by a deformable contour model incorporating region analysis. *Phys Med Biol* **42**:1833–1841.
30. Amini AA, Duncan JS. 1992. Bending and stretching models for lv wall motion analysis from curves and surfaces. *Image Vision Comput* **10**:418–430.
31. Ivins J, Porill J. 1994. Statistical snakes: active region models. In *Proceedings of the fifth British machine vision conference (BMVC'94)*, pp. 377–386. Washington, DC: IEEE.
32. Das B, Banerjee S. 2004. Homogeneity induced inertial snake with applications to medical image segmentation. In *Proceedings of the IEEE Symposium on computer-based medical systems*, pp. 304–309. Washington, DC: IEEE Computer Society.
33. Rougon N, Prêteux F. 1991. Deformable markers: mathematical morphology for active contour models control. *Proc. SPIE* **1568**:78–89.
34. Chakraborty A, Staib LH, Duncan JS. 1994. Deformable boundary finding influenced by region homogeneity. In *Proceedings of the fourth international conference on computer vision (ICCV'94)*, pp. 624–627. Washington, DC: IEEE Computer Society.
35. Chakraborty A, Duncan JS. 1995. Integration of boundary finding and region-based segmentation using game theory. In *Fourteenth international conference on information processing in medical imaging,* pp. 189–200. New York: Kluwer.
36. Herlin IL, Ayache N. 1992. Features extraction and analysis methods for sequences of ultrasound images. *Image Vision Comput* **10**:673–682.
37. Gauch JM, Pien HH, Shah J. 1994. Hybrid boundary-based and region-based deformable models for biomedical image segmentation. *Proc SPIE* **2299**: pp. 72–83.
38. Staib LH, Duncan JS. 1992. Boundary finding with parametrically deformable models. *IEEE Trans Pattern Anal Machine Intell* **14**:1061–1075.
39. Davatzikos CA, Prince JL. 1995. An active contour model for mapping the cortex. *IEEE Trans Med Imaging* **14**:65–81.

40. Cootes TF, Taylor CJ, Cooper D, Graham J. 1995. Active shape models: their training and application. *Comput Vision Image Understand* **61**:38–59.
41. Cootes TF, Edwards GJ, Taylor CJ. 1998. Active appearance models. In *Proceedings of the European conference on computer vision*, Vol. 2, pp. 484–498. New York: Springer.
42. Storvik G. 1994. A Bayesian approach to dynamic contours through stochastic sampling and simulated annealing. *IEEE Trans Pattern Anal Machine Intell* **16**:976–986.
43. Lai KF, Chin RT. 1995. Deformable contours: modeling and extraction. *IEEE Trans Pattern Anal Machine Intell* **17**:1084–1090.
44. Liu L, Sclaroff S. 2001. Medical image segmentation and retrieval via deformable models. In *Proceedings of the international conference on image processing (ICIP'2001)*, Vol. 3, pp. 3–7. Washington, DC: IEEE Computer Society.
45. Olstad B, Torp AH. 1996. Encoding of a priori information in active contour models. *IEEE Trans Pattern Anal Machine Intell* **18**:863–872.
46. Gastaud M, Barlaud M, Aubert G. 2004. Combining shape prior and statistical features for active contour segmentation. *IEEE Trans Circ Syst Video Technol* **14**:726–734.
47. Gunn SR, Nixon MS. 1997. A robust snake implementation: a dual active contour. *IEEE Trans Pattern Anal Machine IntellI* **19**:63–68.
48. Jacob M, Blu T, Unser M. 2004. Efficient energies and algorithms for parametric snakes. *IEEE Transactions on Image Processing* **13**:1231–1244.
49. Das B, Saha PK, Wolf R, Song HK, Wright AC, Wehrli FW. 2005. Cerebrovascular plaque segmentation by using object class uncertainty snake in mr images. *Proc. SPIE* **5747**:1720–1731.
50. Yushkevich PA, Piven J, Cody H, Ho S, Gee JC, Gerig G. 2005. User-guided level set segmentation of anatomical structures with ITK-SNAP. *Insight J* **1** (Special Issue on ISC/NA-MIC/MICCAI Workshop on Open-Source Software, November).
51. Caselles V, Kimmel R, Sapiro G. 1995. Geodesic active contours. In *Proceedings of the fifth international conference on computer vision (ICCV'95)*, pp. 694–699. Washington, DC: IEEE Computer Society.
52. Saha PK, Udupa JK. 2001. Optimum threshold selection using class uncertainty and region homogeneity. *IEEE Trans Pattern Anal Machine Intell* **23**:689–706.
53. Osher S, Sethian JA. 1988. Fronts propagating with curvature dependent speed: algorithms based on Hamilton-Jacobi formulation. *J Computat Phys* **79**:12–49.
54. Malladi R, Sethian J, Vemuri BC. 1995. Shape modeling with front propagation: A level set approach. *IEEE Trans Pattern Anal Machine Intell* **17**(2):158–175.
55. Chan TF, Vese LA. 2001. Active contours without edges. *IEEE Trans Image Process* **10**:266–277.
56. Paragios N, Deriche R. 2000. Geodesic active contours and level sets for the detection and tracking of moving objects. *IEEE Trans Pattern Anal Machine Intell* **22**:266–280.
57. Valdés-Cristerna R, Medina-Bañuelos V, Yáñez-Suárez O. 2004. Coupling of radial-basis network and active contour model for multispectral brain mri segmentation. *IEEE Trans Biomed Eng* **51**:459–470.
58. Samadani R. 1992. Changes in connectivity in active contour models. In *Proceedings of the Workshop on Visualization*, pp. 337–343. Washington, DC: IEEE Computer Society.
59. McInerney T, Terzopoulos D. 1995. Topologically Adaptable Snakes. In *Proceedings of the fifth international conference on computer vision (ICCV'95)*, pp. 840–845. Washington, DC: IEEE Computer Society.
60. McInerney T, Terzopoulos D. 1999. Topology adaptive deformable surfaces for medical image volume segmentation. *IEEE Trans Med Imaging* **18**:840–851.
61. Ji L, Yan H. 2001. Robust topology-adaptive snakes for image segmentation. In *Proceedings of the international conference on image processing (ICIP'2001)*, Vol. 2, pp. 797–800.
62. Lorenson WE, Cline HE. 1987. Marching cubes, a high resolution 3d surface construction algorithm. *Comput Graphics* **21**:163–169.

63. Giraldi GA, Strauss E, Oliveira AA. 2000. A boundary extraction method based on dual-t-snakes and dynamic programming. In *IEEE proceedings of computer vision and pattern recognition (CVPR'2000),* Vol. 1, pp. 44–49. Washington, DC: IEEE Computer Society.
64. Mikić I, Krucinski S, Thomas JD. 1998. Segmentation and tracking in echocardiographic sequences: active contours guided by optical flow estimates. *IEEE Trans Med Imaging* **17**:274–285.
65. Leymarie F, Levine MD. 1993. Tracking deformable objects in the plane using an active contour model. *IEEE Trans Pattern Anal Machine Intell* **15**:617–634.
66. Curwen RW, Amini AA, Duncan JS, Lee F. 1994. Tracking vascular motion in x-ray image sequences with Kalman snakes. *Comput Cardiol,* **1**:109–112.
67. Freedman D, Zhang T. 2004. Active contours for tracking distributions. *IEEE Trans Image Process* **13**:518–526.
68. Ray N, Acton ST, Altes T, Lange EE, Brookeman JR. 2003. Merging parametric active contours within homogeneous image regions for mri-based lung segmentation. *IEEE Trans Med Imaging* **22**:189–200.
69. Ray N, Acton ST. 2004. Motion gradient vector flow: an external force for tracking rolling leukocytes with shape and size constrained active contours. *IEEE Trans Med Imaging* **23**:1466–1478.
70. Gwydir SH, Buettner HM, Dunn SM. 1994. Non-rigid motion analysis and feature labelling of the growth cone. In *Proceedings of the IEEE Workshop on biomedical image analysis,* pp. 80–87. Washington, DC: IEEE Computer Society.
71. Lengyel J, Greenberg DP, Popp R. 1995. Time-dependent three-dimensional intravascular ultrasound. *J Comput Graphics* **29**:457–464.